HHS Public Access

Author manuscript

Cancer Cell. Author manuscript; available in PMC 2025 February 12.

Published in final edited form as:

Cancer Cell. 2024 February 12; 42(2): 266–282.e8. doi:10.1016/j.ccell.2024.01.002.

Inosine Induces Stemness Features in CAR-T cells and Enhances Potency

Dorota D. Klysz[1], **Carley Fowler**[1], **Meena Malipatlolla**[1], **Lucille Stuani**[3], **Katherine A. Freitas**[1], **Yiyun Chen**[1], **Stefanie Meier**[2,5,7], **Bence Daniel**[5,6], **Katalin Sandor**[5], **Peng Xu**[1], **Jing Huang**[1], **Louai Labanieh**[1], **Vimal Keerthi**[1], **Amaury Leruste**[1], **Malek Bashti**[1], **Janette Mata-Alcazar**[1], **Nikolaos Gkitsas**[1], **Justin A. Guerrero**[1], **Chris Fisher**[1], **Sunny Patel**[1], **Kyle Asano**[1], **Shabnum Patel**[1], **Kara L. Davis**[1,3], **Ansuman T. Satpathy**[1,2,5], **Steven A. Feldman**[1], **Elena Sotillo**[1,†], **Crystal L. Mackall**[1,2,3,4,8,†,*]

[1]-Center for Cancer Cell Therapy, Stanford Cancer Institute, Stanford University School of Medicine, Stanford, California

[2]-Parker Institute for Cancer Immunotherapy, San Francisco, California

[3]-Department of Pediatrics, Division of Pediatric Hematology, Oncology, Stem Cell Transplantation and Regenerative Medicine, Stanford University School of Medicine, Stanford, California

[4]-Deparment of Medicine, Division of Bone Marrow Transplantation and Cell Therapy, Stanford University School of Medicine, Stanford, California

[5]-Department of Pathology, Stanford University School of Medicine, Stanford, California

[6]-Center for Personal Dynamic Regul omes, Stanford University, Stanford, California

[7]-Gladstone-UCSF Institute of Genomic Immunology, San Francisco, California

[8]-Lead Contact

Summary

Adenosine (Ado) mediates immune suppression in the tumor microenvironment and exhausted $CD8^+$ CAR-T cells express CD39 and CD73, which mediate proximal steps in Ado generation. Here, we sought to enhance CAR-T cell potency by knocking out CD39, CD73 or adenosine receptor 2a (A2aR), but observed only modest effects. In contrast, overexpression of Ado deaminase (ADA-OE), which metabolizes Ado to inosine (INO), induced stemness and enhanced CAR-T functionality. Similarly, CAR-T cell exposure to INO augmented function and induced

[*]Corresponding author: Crystal L Mackall MD, 265 Campus Drive, Ste 3141A, MC5456, Stanford, CA 94305, 650-725-9670, cmackall@stanford.edu.

Author contributions

C.L.M. supervised the study and acquired funding. D.D.K., E.S. and C.L.M. designed and conceptualized the study. D.D.K cloned the construct, designed and performed experiments, and analyzed data. M.M, L.S., C.F., N.G., J.M-A., M.B., B.D., K.S. performed experiments and collected the data. E.S, K.M, S.M., A.L., Y.C. performed biostatistical analysis. V.K., J.A-G., C.F., P.X., J.H. performed animal experiments and collected the data. A.T.S., S.P., S.F. advised on the experimental design. D.K., E.S., and C.L.M. wrote the manuscript. All other authors commented on and revised the manuscript.

[†]These authors contributed equally: CLM and ES

features of stemness. INO induced profound metabolic reprogramming, diminishing glycolysis, increasing mitochondrial and glycolytic capacity, glutaminolysis and polyamine synthesis, and reprogrammed the epigenome toward greater stemness. Clinical scale manufacturing using INO generated enhanced potency CAR-T cell products meeting criteria for clinical dosing. These results identify INO as a potent modulator of CAR-T cell metabolism and epigenetic stemness programming and deliver an enhanced potency platform for cell manufacturing.

Graphical Abstract

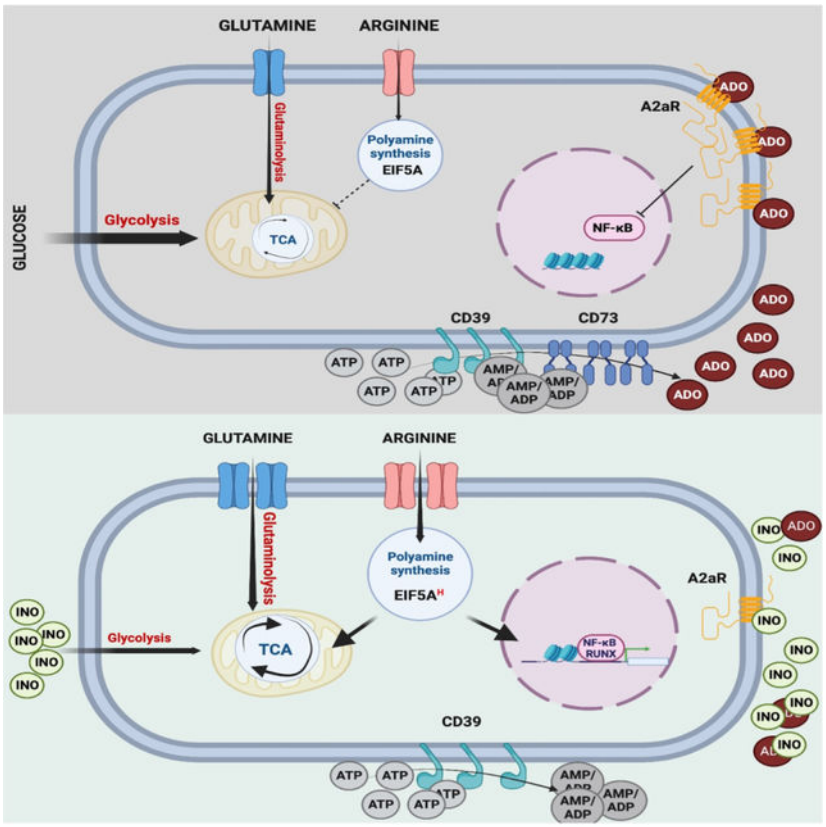

In brief

Klysz et al show that targeting CD39, CD73 or A2aR doesn’t reduce adenosine-mediated immunosuppression, but increasing inosine levels, by direct supplementation or overexpression of adenosine deaminase, augments CAR-T cell function and stemness. Introduction of inosine during GMP cell manufacturing process is a feasible strategy to generate more potent CAR-T cell.

INTRODUCTION

Adenosine (Ado) is an immunosuppressive nucleoside that contributes to immune evasion in the tumor microenvironment (TME). CD39 (ecto-ATP diphosphohydrolase-1, *ENTPD-1*) and CD73 (5′-ectonucleotidase, *NT5E*), metabolize ATP to Ado, which mediates immunosuppression primarily via A2aR signaling[1]. Murine $CD4^+$ Tregs co-express CD39 and CD73 and mediate immunosuppression, in part, through production of Ado[2]. In humans,

CD39 is expressed by most Tregs, and CD73 expression can be induced by hypoxia-inducible factor 1-alpha, HIF1a[3–5]. In the TME, tumor-reactive T cells are enriched in the $CD39^+$ subset[6–8]. Although several studies have correlated improved prognosis with higher numbers of $CD39^+$ tumor infiltrating lymphocytes[7,9–11], functional studies demonstrate that CD39 marks dysfunctional, exhausted T cells[12–15].

Chimeric antigen receptors (CARs) link extracellular antigen binding domains to intracellular signaling domains, enabling MHC-independent antigen-specific T cell reactivity[16]. CAR-T cells are highly effective against refractory B cell malignancies but less potent against solid tumors and exhaustion is a major factor limiting the potency of CAR-T cells[17–23]. Here we interrogated the biology of CD39 and the role of Ado in the dysfunction of exhausted human T cells and sought to enhance CAR-T cell potency by engineering adenosine resistance. Using an *in vitro* model of human CAR-T cell exhaustion, we observed that exhausted $CD8^+CD39^+$ T cells co-express CD73, generate Ado, and mediate Ado-related suppression via A2aR[14,24]. To induce Ado resistance, we knocked out CD39, CD73 or A2aR, but observed only modest phenotypic and transcriptional changes. In contrast, overexpression of membrane tethered adenosine deaminase (ADA), which metabolizes Ado to inosine (INO), significantly altered the transcriptome toward stemness and enhanced the fitness of CAR-T cells. Similarly, exposure of CAR-T cells to INO induced a stemness-associated gene expression program and augmented CAR-T cell function.

Single cell profiling revealed that INO reprograms the metabolome, decreasing glycolysis, but increasing glutaminolysis, polyamine synthesis and oxidative phosphorylation. These effects are associated with epigenetic reprogramming towards stemness. Clinical scale manufacturing using INO-supplemented media generated CAR-T cell products meeting criteria for clinical dosing that demonstrated enhanced potency in animal models. These data identify INO as an inducer of CAR-T cell stemness and provide evidence that nutrient modulation can drive epigenetic changes that regulate T cell differentiation and enhance T cell fitness.

RESULTS

CD39 marks a subset of human exhausted CAR-T cells with diminished functionality and hallmark features of regulatory T cells.

To assess the biology of CD39 in the context of human CAR-T cell exhaustion, we studied kinetics of CD39 expression vs other canonical exhaustion markers on T cells expressing the GD2-targeting tonically signaling HA-CAR, previously described to induce T cell exhaustion within 10 days post-activation *in vitro*[14,24]. As controls for HA-CAR-T cells, we used CD19-CAR T cells, which do not tonically signal and are not predisposed to exhaustion, as well as HA-CAR-T cells cultured in the presence of dasatinib, a tyrosine kinase inhibitor that blocks CAR signaling, preserving CAR-T cell fitness[24]. PD-1, TIM-3, and LAG3 were upregulated on essentially the entire population of HA-CAR-T cells by day 4 following activation and remained elevated as HA-CAR cells transition to exhaustion, whereas CD39 demonstrated limited upregulation early after activation, gradually increasing on a subset of cells as they transition to exhaustion (Figure 1A). We observed a higher

frequency of CD39 expression on CAR^+ vs. CAR^- cells (Figure 1B) and, CD39 was preferentially upregulated on $CD8^+$ vs. $CD4^+$ T cells (Figure 1C, S1A). Following antigen exposure, $CD39^+CD8^+$ secreted lower levels of IL-2 compared to their $CD39^-$ counterparts (Figure 1D), but produced more TGFβ and IL-27, cytokines associated with suppressive T cells[25–27].

$CD39^+$ CAR-T cells also demonstrated distinct transcriptomic profiles compared to $CD39^-$ subsets, with higher levels of exhaustion/effector-related genes (*NR4A1-A3*, and *KLRD1*)[28], increased Treg-associated genes (*FOXP3, TIGIT, IL2RA, RXRA)*[29], and lower expression of genes that drive stemness such as *TCF7, TCF4, SELL, LEF1* and *IL-7R* (Figure S1B). These findings were confirmed by Gene Set Enrichment Analysis (GSEA), which demonstrated that $CD39^+CD8^+$ and $CD4^+$ CAR-T cells resemble both exhausted T cells and $CD4^+$ regulatory T cells (Figure 1E, S1C), whereas $CD39^-$ CAR-T cells resemble non-exhausted CAR-T cells[24,30]. Mass cytometry (CyTOF) confirmed higher levels of exhaustion-associated (TIM-3, PD-1, LAG3) and suppression-associated proteins (Foxp3, TIGIT, CD49b, LAP, CD73, CTLA4) in $CD39^+$ vs. $CD39^-$ HA-CAR-T cells (Figure 1F).

The $CD39^+$ subset could represent expansion of a preexisting $CD39^+$ population or CD39 induction in response to tonic signaling. To distinguish between these possibilities, we sorted $CD39^-$ HA-CAR-T cells and cultured them ± dasatinib, then assessed CD39 expression (Figure S1D)[14,31]. $CD39^-$ HA-CAR cells rapidly re-expressed CD39, which was prevented by dasatinib, confirming a requirement for CAR signaling to upregulate CD39 in this model. TGFβ contributes to CD39 upregulation in regulatory T cells, but neutralizing anti-TGFβ antibody did not affect the frequency of $CD39^+$ cells, nor expression levels of CD39 on HA-CAR-T cells in this system[32]. Together, these data demonstrate that CD39 expression is induced by chronic T cell activation and marks a highly dysfunctional subset of exhausted CAR-T cell with hallmark features of regulatory T cells.

A high fraction of exhausted $CD39^+$ CAR-T cells co-express CD73, generate Ado and mediate immunosuppression through A2aR.

CD39 metabolizes extracellular ATP (eATP) to ADP/AMP and these are metabolized by CD73 to Ado, which signals via A2aR to induce 3',5'-cyclic Ado monophosphate (cAMP) and can inhibit NF-κB (Figure 1G)[33]. We observed increased frequencies of $CD39^+CD73^+$ co-expression in exhausted HA-CAR-T cells compared to CD19-CAR or mock non-transduced T cells (Figure 1H). The frequency of $CD39^+CD73^+$ cells was significantly higher in $CD8^+$ vs. $CD4^+$ HA-CAR-T cells. CD39 and CD73 are enzymatically active on exhausted HA-CAR-T cells since they induced greater eATP hydrolysis (Figure 1I) and generated more Ado than mock or control CD19-CAR-T cells (Figure 1J). Knockout of CD39 or CD73 from HA-CAR-T cells (HA-CD39KO and HA-CD73KO) (Figure S1E), confirmed the requirement for CD39 to hydrolyze eATP to ADP/AMP, and for CD39 and CD73 to generate Ado in this system (Figure 1I, 1J).

To test whether CAR-T cells are susceptible to Ado-mediated suppression, we activated HA- or CD19-CAR-T cells with antigen, in the presence or absence of the Ado receptor agonist 5′-(N-ethylcarboxamido) adenosine (NECA). NECA reduced antigen-induced IL-2 production (Figure S1F), but this inhibition was prevented by CPI-444, a selective A2aR

competitive antagonist (iA2aR)[34]. To assess whether $CD8^+$ HA-CAR-T cells mediate immune suppression and if this is mediated by Ado, we stimulated CD19-CAR-T cells in the presence of bulk HA-CAR-T cells or sorted $CD8^+$ HA-CAR-T cells and observed decreased antigen-induced IL-2 production by CD19-CAR-T cells (Figure S1G). CD39 expression was required by the suppressor population and A2aR expression in the responder population for the immunosuppressive effect (Figure 1K). Despite reduced Ado generation and reduced suppression by CD39KO, we saw no change in cytotoxic potency between CD39KO and control CAR-T cells against solid mg63.3 or leukemia Nalm6-GD2 tumor lines (Figure S1H, S1I). Together, data demonstrate that $CD39^+$ exhausted CAR-T cells mediate immunosuppression via Ado.

Overexpression of Ado deaminase (ADA-OE) induces transcriptomic and phenotypic features of T cell stemness.

With the goal of developing a cell intrinsic approach to prevent Ado mediated immunosuppression, we assessed phenotypes of CD39KO and CD73KO CAR-T cells and A2aRKO HA-CAR-T cells. Reasoning that adenosine deaminase catabolizes Ado to INO, reducing Ado-mediated immunosuppression, we also incorporated an experimental group with membrane tethered overexpression of ADA (ADA-OE) (Figure 2A, S2A). All groups showed similar CAR expression levels (Figure S2B). Principal component (PCA) and differential gene expression analyses showed that ADA-OE induced the most significant transcriptional changes compared to control, while all KO versions of the HA-CAR were more similar to the control (Figure 2B, 2C). Compared to controls, ADA-OE induced upregulation of genes associated with stemness (*TCF7, IL-7R, SELL*) and downregulation of genes associated with effector function (*GZMB, IFNγ*, *TNFSF4*) and exhaustion (*LAG3, CTLA4, HAVCR2, TOX2, TOX* or *PDCD1*) (Figure 2D, S2C). Expression of these genes in CD39KO or CD73KO seemed to be intermediate between exhausted control HA-CAR-T cells and ADA-OE cells, showing partial downregulation of effector function genes, subtle upregulation of stemness-associated genes and variable changes in genes associated with exhaustion (Figure 2D). Accordingly, GSEA analysis of ADA-OE HA-CAR-T cells showed negative enrichment with sets associated with T cell exhaustion and a positive enrichment with sets of non-exhausted CD19-CAR-T cells and CD19-CAR-T cells associated with long-term complete response (Figure S2D)[24,30,35].

To assess whether the transcriptomic changes observed translated to protein expression, we used CyTOF to evaluate a panel of 26 surface markers and transcription factors (TFs) (Figure 2E). Consistent with the transcriptomic analysis, ADA-OE $CD8^+$ and $CD4^+$ HA-CAR-T cells were most distant from controls, showing higher expression of stemness markers (CD27, CD45RA and CD127), and lower expression of exhaustion (LAG3, PD-1, T-bet, TOX) and activation (CD25 and 4–1BB) markers (Figure 2F, S2E). FlowSOM analysis[36] of $CD8^+$ ADA-OE vs. control HA-CAR-T cells revealed increased frequencies of stem-like memory T cells (SCM) ($CCR7^{++}CD127^+CD95^+CD62L^+CD45RA^{++}LEF1^{++}$), and decreased progenitor exhaustion (Pexh) ($TCF1^{++}TOX^+T\text{-}bet^+LEF1^+CD45RO^+Ki67^+PD\text{-}1^+$ $^+LAG3^{++}TIM\text{-}3^+4–1BB^+$) and terminally differentiated exhausted-like (Exh) ($TCF1^+$ $^+TOX^+T\text{-}bet^{++}LEF1^+CD45RO^+Ki67^+PD\text{-}1^+LAG3^+TIM\text{-}3^+4–1BB^-$) populations (Figure 2G)[37,38]. Similar findings were seen in $CD4^+$ ADA-OE cells compared to control HA-CAR-

T cells (Figure S2F–G). CD39KO and CD73KO cells manifested an intermediate phenotype with reduced fractions of Pexh cells, no change in frequency of Exh cells compared to control, but increased fractions of stem-like memory T cells and effector subsets (EF) ($CD38^{++}TCF1^{+}T\text{-}bet^{+}CD45RO^{+}CD45RA^{-}PD\text{-}1^{-}LAG3^{lo}TIM\text{-}3^{lo}4\text{–}1BB^{-}CCR7^{-}$). No significant difference was observed in the frequency of effector memory-like cells (EM) ($CD38^{lo}TCF1^{+}T\text{-}bet^{+}CD45RO^{lo}CD45RA^{-}PD\text{-}1^{-}LAG3^{lo}TIM\text{-}3^{lo}4\text{–}1BB^{-}CCR7^{lo}$) (Figure 2G). Together, the data demonstrate that ADA-OE, and to a lesser extent CD39KO or CD73KO but not A2aRKO, induces transcriptomic and phenotypic features of stemness, raising the prospect that ADA-OE could be inducing effects beyond inhibition of Ado signaling and related to the generation of INO, which T cells can use as an alternative energy source to glucose for metabolic processes[39].

INO increases stemness features, enhances CAR-T cell functionality, and abrogates immune suppression in chronically activated CAR-T cells independently of the presence of glucose.

To test if INO could modulate stemness in chronically activated CAR-T cells, we activated, transduced and cultured cells in standard RPMI containing 11mM of glucose (unchanged from previous experiments) and, on day 4, split cultures into standard RPMI or RPMI containing 11 mM of INO, without glucose (HA-INO-CAR) (Figure 3A). Transcriptomic analysis on day 14 demonstrated that HA-INO-CAR-T cells manifested differential expression of >3,000 transcripts compared to cells expanded in control media (PC1 variance 41.3%, Figure 3B). CAR-T cells cultured in INO exhibited increased expression of equilibrative nucleoside transporters 1 (ENT1), whereas ENT2 was significantly downregulated together with genes involved in the purinergic pathway *NT5E* (CD73), *ADORA2A* (A2aR), and FOXP3 T cells (Figure S3A). GSEA analysis demonstrated that HA-INO-CAR-T cells upregulated transcriptional programs associated with stem cell-like memory (Figure 3C). Accordingly, flow cytometry following INO exposure demonstrated higher levels of CD62L (Figure S3B) and we confirmed by CyTOF higher levels of protein expression of stemness markers (CD45RO, CCR7, CD127) in $CD8^{+}$ and $CD4^{+}$ HA-INO-CAR-T cells (Figure S3C).

Functional studies following challenge with tumor cell lines expressing high (Nalm6-GD2) or low (143B) levels of GD2 (Figure S3D) revealed increased cytotoxicity and cytokine production by both ADA-OE and HA-INO-CAR vs. control HA-CAR-T cells (Figure S3E–F), with HA-INO-CAR-T cells showing highest potency. Cytokine secretion was also greater for CD19-INO-CAR-T cells than control or ADA-OE CD19-CARs when challenged with Nalm6 presenting low levels of CD19, which is a major cause of resistance to CAR-T cells[40] (Figure S3D–F). We also confirmed that HA-INO-CAR-T cells lack immunosuppressive capacity we previously observed in HA-CAR-T cells (Figure S3G). Decreased A2aR gene expression together with improved effector function raised the prospect that INO exposure could diminish susceptibility to Ado-mediated immunosuppression. To test this, we co-cultured HA- and HA-INO-CAR-T cells with Nalm6-GD2 in increasing concentrations of Ado (Figure S3H). HA-CAR-T cells were maximally suppressed, as measured by IFNγ inhibition, with 40uM of Ado, whereas the same concentration had marginal effects on HA-INO-CAR-T cells. A similar trend was observed in CD19-CAR-T cells. These data

suggest that INO not only induces stemness and increases effector function but also protects against adenosine mediated suppression.

Transcriptomic and epigenetic hallmarks of exhaustion occur within 10–12 days in the HA-CAR model[24]. To determine if INO can induce a stem-like phenotype in already exhausted T cells, we exposed HA-CAR-T cells to INO on days 4, 7, 10 and 14 post-activation, analyzing phenotype and function (Figure 3D). We observed increased frequencies of $CD8^+CD62L^+$ HA-CAR-T cells and increased cytotoxic function regardless of when INO was added, providing evidence that INO can enhance stemness even in cells already manifesting features of exhaustion (Figure 3E, 3F). Similarly, enhanced cytotoxic function in response to challenge with Nalm6-GD2 tumor was observed in non-exhausted CD19-CAR-T cells following exposure to INO (Figure S3I).

We next sought to determine whether INO mediated augmentation of T cell function could be attributed to glucose deprivation[41]. HA-CAR-T cells were cultured from day 4 post-activation in control media containing glucose and/or, INO or in starvation for both. We observed that any condition including INO showed diminished expansion (Figure 3G), enhanced CD62L expression (Figure 3H), higher frequency of central memory (CM) cells (Figure S3J) and enhanced antigen induced IFNγ secretion (Figure 3I), demonstrating that the effects observed could not be attributed to glucose deprivation. Furthermore, while glucose deprivation induced a similar reduction in expansion compared to INO supplementation, it did not induce significant levels of CD62L, CM cell expansion or enhanced antigen-specific activation.

We next titrated INO concentration between 0–11mM in regular RPMI containing glucose and observed a clear dose-dependent effect on diminished proliferation, increased CD62L expression and increased antigen induced IFNγ production with increasing INO concentration without a plateau (Figure 3J–L). Similarly, decreased cell proliferation in the media containing INO, but not glucose, was proportional to the time cells were exposed to INO (Figure S3K). Decreased proliferation can be associated with induction of stemness or cells entering quiescent state[42,43]. Analysis of the cell cycle revealed that INO-CAR-T cells had a lower proportion of cells in G1 phase as compared to control cells (Figure 3M, S3L), supporting the hypothesis that INO promotes stemness retention in proliferating CAR-T cells rather than causing quiescence. Measurement of viability and antigen-induced expansion of HA-INO or HA-CAR-T cells after co-culture with Nalm6-GD2 or 143B tumor cells showed no differences in CAR-T cell viability, but greater expansion of HA-INO cells post-activation (Figure S4A–B). Finally, we confirmed that functional enhancements endowed by INO happened regardless of whether glucose was present or absent during the CAR-T cell manufacturing process (Figure S4C, S4D). Together these data demonstrate that INO restrains proliferation of activated CAR-T cells, induces a more stem-like phenotype, endows enhanced functionality, and eliminates suppressive activity. These effects occur independently of glucose, and only the diminished expansion is replicated by glucose deprivation.

CAR-T cells cultured in inosine mediate superior tumor control *in vivo*

To test the effect of INO and ADA-OE on CAR-T cell function *in vivo*, we treated Nalm6 bearing mice with suboptimal doses of CD19-CAR T cells. Both INO cultured and ADA overexpressing CD19-CAR-T cells significantly extended mice survival time (Figure S5A–B). We next conducted a "stress test" using suboptimal doses of HA-CAR-T cells in the Nalm6-GD2 leukemia model (Figure 4A) and observed delayed tumor growth and increased overall survival in HA-INO- vs. HA-CAR-T cells (Figure 4B–C). CD19-INO-CAR-T cells also manifested enhanced capacity to control antigen low tumor cells *in vitro* compared to control and ADA-OE CD19-CARs (Figure S5B–S5C) and INO-treated CD19-CAR-T cells also exhibited increased anti-tumor activity *in vivo* in a stress test against CD19 leukemia (Figure 4D–E).

Finally, we tested efficacy of INO-CAR-T cells in a Her2-CAR, which has been used by others to study Ado-related immunosuppression[44], in the 143B osteosarcoma model (Figure 4F). Tumors treated with mock or Her2-CAR-T cells grew at the same rate, whereas Her2-INO-CAR-T cells prevented tumor growth and prolonged survival (Figure 4G–H, S5C). We observed 10 times more circulating T cells in the blood of mice 17 days after receiving the Her2-INO-CAR vs control Her2-CAR-T cells (Figure 4I). Together, these results demonstrate that exposure to INO during CAR manufacturing enhances antitumor potency of both exhaustion-prone HA-CAR-T cells and non-exhaustion prone CD19-CAR-T cells, and these cells also manifest enhanced antitumor potency and enhanced CAR-T cell persistence in a challenging solid tumor model.

Inosine modifies metabolic programming of chronically activated CAR-T cells

To explore the effects of INO on CAR-T cell metabolism, we conducted DAVID gene annotation enrichment analysis using KEGG pathways and GO terms (Figure 5A) and observed evidence for metabolic reprogramming, with downregulation of genes associated with glycolysis and glucose driven metabolism (*PFKP*, *ALDOA*, *GAPDH*, *PGK*, *ENO1*), and increased expression of genes associated with glutaminolysis and polyamine synthesis (Figure 5B–C). INO increased expression of ornithine decarboxylase (ODC), the proximal, rate limiting enzyme for putrescine synthesis and spermidine synthase, which generates spermidine and eIF5A, important mitochondria activity regulators. These metabolic effects were associated with diminished expression of genes associated with TCR signaling consistent with decreased effector differentiation.

To confirm these findings, we conducted single cell proteomics via CyTOF (Figure 5D)[45], which demonstrated reduced levels of enzymes associated with glycolysis, including reduced hexokinases (HK1/2), glyceraldehyde 3-phosphate dehydrogenase (GAPDH), enolase 1 (ENO1) and PKM2 in HA-INO- vs. control CAR-T cells. Importantly, glycolysis was not completely inhibited, since glycolytic enzymes were present at similar levels in HA-INO- vs. control CD19-CAR-T cells, consistent with previous evidence demonstrating that INO is capable of providing a carbon source for glycolysis[39]. INO cultured cells also expressed higher levels of enzymes associated with glutaminolysis (GLS, GPT2), and TCA activity (IDH1, IDH2, CS, SDHA), consistent with INO induced glutamine catabolism driving TCA through anapleurosis (Figure 5D). Proteins of complex I and V of the electron

transport chain were also elevated, consistent with higher oxidative phosphorylation. Expression of CAT2, a high efficiency transporter of the polyamine precursor-arginine also increased following INO culture, furthering confirming increased polyamine synthesis (Figure 5D)[46].

To measure mitochondrial fitness in INO-CAR-T cells, we performed Seahorse analysis. Basal oxygen consumption rate (Basal OCR) did not differ between control and INO cultured cells, however HA-INO-CAR-T cells exhibited increased maximal OCR and spare respiratory capacity (SRC), both hallmarks of memory-like cells (Figure 5E–5F). This effect was maintained even when cells were cultured in the presence of both INO and glucose indicating a dominant and specific effect of inosine. Of note, INO induced a memory-like metabolic profile in non-tonic signaling CD19-CAR-T cells (Figure S6A). To directly measure the effect of INO on glycolytic function, we performed a Seahorse Glycolytic Stress Test (Figure 5G), which revealed no differences in glycolysis at baseline, however HA-INO cells exhibited significantly increased glycolytic capacity and reserve when mitochondrial activity was blocked by oligomycin (Figure 5H). These results indicate that INO increases T cell resistance to oxidative stress and enables more efficient use of glycolysis to compensate for energetic needs when oxidative phosphorylation is not available. The increase in the metabolic activity correlated with an increased size of the cells in INO condition (Figure S6B).

Together, phenotypic, transcriptomic, and proteomic profiling demonstrate that INO induces stemness programming and augmented functionality and is associated with profound metabolic reprogramming, characterized by diminished glycolysis, increased glutaminolysis and polyamine synthesis, increased TCA and mitochondria activity and glycolytic reserve.

Inosine modulates the epigenetic landscape toward stemness

T cell exhaustion is associated with widespread epigenetic changes and mμetabolic pathways have been implicated in modulating the T cell epigenome[14,24,47–49]. To assess whether INO-induced functional and metabolic reprogramming is associated with epigenetic reprogramming, we performed ATAC-seq on $CD8^+$ HA- and HA-INO-CAR-T cells. INO induced widespread changes in chromatin accessibility spanning more than 10,000 genomic regions (PC1 variance 57%) (Figure 6A–B), with enhanced chromatin accessibility in regulatory regions associated with IL-2 and several stemness genes (*TCF7, IL-7R, CCR7* and *CXCR3*) (Figure 6C). ChromVAR and HOMER transcription factor binding motif enrichment analysis demonstrated that INO also increased accessibility of RUNT (RUNX1/2), IRF (IRF1/2/3/4/8, ISRE) and RHD (NFKB1/2, REL(A)) family TF binding motifs, which are associated with memory differentiation[50] (Figure 6D). In contrast, accessibility of cAMP-response element binding proteins CREB1 and ATF7 were decreased in INO-HA compared to HA-CAR-T cells, raising the prospect that INO exposed cells are less susceptible to Ado-mediated suppression (Figure 6E). Previous work has implicated polyamines in epigenetic regulation of Th1 differentiation through hypusination of translation elongation factor EIF5A. We observed increased expression of EIF5A in HA-INO-CAR-T cells suggesting that a similar pathway may be involved in INO induced epigenetic programming (Figure 6F)[47,51]. To test whether EIF5A hypusination mediated

INO reprogramming in our model, we used ciclopirox (CPX), a small molecule that inhibits the deoxyhypusine hydroxylase (DOHH) enzyme required for EIF5A hypusination (Figure 6G) and observed a striking decrease in frequency of CM-like cells (Figure S7A). To further validate these findings, we knocked-out EIF5A using CRISPR/Cas9 (Figure 6H) and observed loss of the INO effect, since EIF5AKO HA-CAR-T cells exhibited phenotypes similar to control HA-CAR-T cells when cultured in INO. Together, data demonstrate that INO induces stemness by metabolic and epigenetic programming via modulation of polyamine metabolism and hypusination of EIF5A.

Large scale manufacturing of clinical grade GD2-CAR-T cells using inosine-containing media improves CAR product quality.

We next assessed feasibility of supplementing INO in a GMP manufacturing workflow, at clinical scale, using GD2-CAR-T cells currently on clinical trial for diffuse midline gliomas (DMGs).[52]. A total of 2.5×10^8 enriched healthy donor $CD4^+$ and $CD8^+$ T cells were activated with anti-CD3/CD28 beads and transduced using clinical grade GD2-CAR vector at 10 MOIs (Figure 7A). On day 3, T cells were maintained in standard RPMI media containing glucose or switched to INO-RPMI without glucose in a semi-closed G-Rex culture platform. On day 7, there was no difference in transduction efficiency, CD4/CD8 ratio or viability between control and INO-CAR-T cells (Figure 7A). Total cell yield in INO cultures was reduced compared to control cultures as predicted ($238.5\times10^6\pm145.8$ vs. $387.7\times10^6\pm165$s.e.m., respectively), however, yields were sufficient to formulate clinical doses of 1×10^6 CAR-T cells/kg body weight (+/−20%) (Figure 7B). Consistent with the results from the small-scale experiments, we observed a higher frequency of naive and CM GD2-CAR-T cells in INO cultures (Figure S8A). When stimulated with 143B (low GD2 expression), mg63.3 or Nalm6-GD2 (high GD2 expression) tumor cells, GD2-INO-CAR-T cells secreted significantly more IL-2 and IFNγ (Figure 7C), mediated significantly greater antitumor effects *in vivo* (Figure 7D), and exhibited greater persistence when compared to control GD2-CAR-T cells (Figure 7E).

To test compatibility of adding INO to GMP-grade culture media that contains glucose, we manufactured GD2-CAR-T cells in TexMACS™ with increasing concentrations of INO (Figure 7F) and observed significantly decreased cell proliferation (Figure S8B) but no changes in CAR-T cell viability (Figure S8C). INO increased CD62L expression compared to control cells (Figure S8D) and increased secretion of IL-2 and IFNγ when cells were challenged with 143B cells (Figure 7G). While INO concentrations between 5–11mM mediated similar anti-proliferative effects and CD62L induction, we observed a trend toward greater antigen induced cytokine production with INO concentrations of 11mM (Figure 7G). Together, these data demonstrate that CAR-T cells can be manufactured in INO containing media using a GMP adaptable process to reach clinically relevant doses that meet standard release criteria and that such cells demonstrate enhanced functionality compared to those manufactured using standard glucose-based media.

DISCUSSION

Ado is a potent immunosuppressant in the TME and substantial efforts are underway to inhibit Ado to enhance antitumor immune responses[53]. CD39 mediates an early step in Ado generation and is expressed by regulatory T cells and exhausted tumor-reactive T cells in the TME[2,8,9,13,33,54]. Here, we interrogated the biology of CD39 and Ado in the context of T cell exhaustion and observed that CD39 marks a highly dysfunctional subset of exhausted $CD8^+$ T cells that commonly express CD73, manifest phenotypic characteristics of suppressive T cells, and mediate immune suppression via Ado production and signaling via A2aR.

Knockout of CD39, CD73 or A2aR induced modest changes in exhausted CAR-T cells, whereas ADA-OE, increased frequencies of stem cell memory subsets and diminished progenitor exhausted and exhausted subsets, similar to findings reported with overexpression of collagen binding ADA[53,55]. ADA-OE, but not CD39-, CD73- or A2aR-KO, also induced transcriptional reprogramming that augmented expression of stemness associated genes. Together these results implicated INO, the metabolically active product of ADA catabolism in stemness programming of CAR-T cells.

INO is a multifunctional intra- and extracellular purine that serves as a carbon source for bioenergetics in human T cells, is integrated into tRNA where it plays an important role in gene translation and can signal via A2aR and potentially other adenosine receptors[39,56]. *Bifidobacterium pseudolongum* derived INO augments the effectiveness of anti-CTLA4 therapy in humans and mice via A2aR and IFNγ-dependent induction of Th1 differentiation[57]. In murine models where tumors are unable to utilize INO for bioenergetics, systemic INO augmented the efficacy of anti-CTLA4 and GD2-CAR-Therapy[39]. In addition to its immune activating effects, dendritic cell generation and release of INO via a FAMIN dependent pathway prevented autoimmunity and autoinflammation in murine models[58]. Thus, there is accumulating evidence for immunomodulatory effects of INO but mechanistic understanding of its effects in T cells has remained difficult to pinpoint given its pleiotropy.

Nucleosides, such as Ado and INO, are transported across membranes through equilibrative nucleoside transporters 1 and 2 (ENT1 and ENT2)[59]. Based on levels of RNA expression, our data suggest that ENT1 is the main INO transporter in CAR-T cells. INO dramatically enhanced transcription of gene programs associated with stemness and downregulated genes involved in purinergic signaling (CD39, CD73 and A2aR), which was associated with increased adenosine-resistance and significantly enhanced effector function of CAR-T cells. Ado signaling via A2aR upregulates Foxp3[60] while here we observed INO induced downregulation of ADORA2A and FOXP3 expression demonstrating distinctive programming between Ado and INO. Metabolic pathways can play a central role in programming T cell differentiation and function and can be regulated by nutrient availability[61–64]. Consistent with this, INO diminished T cell proliferation, and reprogrammed the metabolome toward diminished glycolysis, increased glutaminolysis, polyamine synthesis and mitochondrial and glycolytic reserve capacity.

While some effects of INO, such as reduced glycolysis and diminished proliferation, overlap with effects seen with transient glucose restriction, the stemness programming effects of INO are distinct and INO induced stemness and metabolic programming was observed regardless of glucose when tested at physiologic levels (5–18mM)[41]. A notable effect of INO in this system was augmentation of polyamine synthesis, with significant induction of ornithine decarboxylase, the rate limiting enzyme in generating spermatine, SRM, and EIF5a. Glutaminolysis was also increased by INO and can also drive induction of polyamines synthesis[65]. Increased polyamine levels have been implicated in regulating the TCA cycle via EIF5A hypusination and in inducing chromatin remodeling during Th1 differentiation in mice[47,66]. The frequency of CM-like HA-CAR-T cells was diminished upon EIF5A knockdown, and following treatment with a hypusination inhibitor, implicating polyamine metabolism in INO-dependent induction stemness programming. INO induced metabolic reprogramming also drove major changes in chromatin accessibility, increasing availability of TF motifs associated with T cell memory and diminishing accessibility of motifs associated with T cell activation. Together, the data support a model wherein INO induced metabolic programming drives polyamine synthesis, which in turn augments oxidative phosphorylation and leads to epigenetic programming of T cells toward stemness.

These observations were readily translated into a clinical scale platform for CAR-T cell manufacturing. GD2.BBz-CAR-T cells mediate activity in patients with diffuse midline glioma but their potency is been limited by tonic signaling and early exhaustion[17,23,24]. Here we show feasibility and enhanced potency of CAR-T cells manufactured in INO containing media. Although the magnitude of T cell expansion was diminished compared to control cultures, sufficient cell numbers were manufactured in 7 days to meet clinical dosing guidelines. Recent studies have suggested that lower doses of CAR-T cells manufactured to retain stemness features may be superior to higher doses of cells manufactured using current standard approaches[67]. GD2-CAR-T cells manufactured in INO manifested a more memory-like phenotype, with higher frequencies of naïve and memory populations compared to control, and increased effector function *in vitro* and *in vivo*.

In summary, these data demonstrate that INO is a potent inducer of T cell stemness that dramatically modulates T cell metabolism, augments function and induces epigenetic programming. INO can be used to manufacture cell products with enhanced potency compared to standard glucose-based media. While many approaches are under development to inhibit Ado generation or signaling, our data suggest that approaches designed to metabolize Ado in the TME and generate INO may prove to be more effective in augmenting antitumor immunity.

STAR METHODS

RESOURCES AVAILABILITY

Lead contact—Further information and requests for resources should be directed to and will be fulfilled by the lead contact, Crystal L. Mackall (cmackall@stanford.edu).

Materials availability—Plasmids generated in this study will be made available upon request and completion of a Material Transfer Agreement.

Data and code availability—The RNaseq and ATACseq datasets generated during this study are available at GEO GSE250443 [https://www.ncbi.nlm.nih.gov/geo/query/acc.cgi?acc=GSE250443].

Details of the analysis are provided in the STAR Methods section. Any additional questions should be directed to and will be fulfilled by the lead contact.

EXPERIEMENTAL MODEL AND SUBJECT DETAILS

Source of primary human T cells—Buffy coats from healthy donors were purchased from the Stanford Blood Center under an IRB-exempt-protocol. Primary human T cells were purified by negative selection using the RosetteSep Human T cell Enrichment kit (STEMCELL Technologies) and SepMate-50 tubes. Fresh Leukopaks from healthy donors were obtained from STEMCELL Technologies and processed for positive selection using the CliniMACS GMP MicroBeads (Miltenyi). T cells were cryopreserved at 1–2×107 cells per mL in CryoStor CS10 cryopreservation media (STEMCELL Technologies) until use.

Cell lines—The Nalm6-GL B-ALL cell line was provided by Dr. D. Barrett (Children's Hospital of Philadelphia). Nalm6-GD2 was created by co-transducing Nalm6-GL with cDNAs for GD2 synthase and GD3 synthase.

All cell lines were cultured in CM RPMI. STR DNA profiling of all cell lines is conducted by Genetica Cell Line testing once per year. None of the cell lines used in this study is included in the commonly misidentified cell lines registry.

Animal models—NOD-SCID-Il2rg−/− (NSG) mice were purchased from JAX, bred in-house and treated in ethical compliance with Stanford University IACUC (APLAC) approved protocols. Six-to-eight-week-old male or female mice were inoculated with either 1×10^6 Nalm6-GL leukemia via intravenous or 1×10^6 143B osteosarcoma via intramuscular injections. All CAR-T cells were injected intravenously and media swap to inosine-supplemented media was performed at day 6 post activation. Time and treatment dose are indicated in the figures. Bioluminescence imaging was performed using a Spectrum IVIS instrument. Values were analyzed using Living Image software. Solid tumor progression was followed using caliper measurements of the injected leg area. Mice were humanely euthanized when an IACUC-approved end-point measurement reached 1.75cm in either direction or when mice demonstrated signs of morbidity and/or hind-limb paralysis. Mice were randomized to ensure equal pre-treatment tumor burden before CAR-T cell injection.

METHOD DETAILS

Viral vector construction—MSGV retroviral vectors encoding the following CARs were previously described: CD19–28z, CD19-BBz, GD2-BBz and Her2-BBz. HA-CAR was created as previously described in[24] by introduction of a point mutation into the 14G2a scFv of the GD2–28z-CAR plasmid to create the E101K mutation.

CAR-T cell production—Non-tissue culture treated 12-well plates were coated ON at 4°C with 1ml Retronectin (Takara) at 25μg/ml in PBS. Plates were washed with PBS and blocked with 2% BSA for 15min. Retroviral supernatant was added at approximately 1ml

per well and centrifuged for 2h at 32°C at 400g before the addition of cells. Primary human T cells were activated with Human T-Expander CD3/CD28 Dynabeads (Gibco) at a 3:1 bead:cell ratio in complete (CM) RPMI 1640 supplemented with 10% fetal bovine serum, 10 mM HEPES, 2 mM GlutaMAX, 100 U/mL penicillin (Gibco), and 100 U/mL IL-2 (Peprotech). T cells were transduced with retroviral vector on day 2 post-activation. Beads were taken off at day 4. In INO condition, after removing activation beads, CAR-T cells were centrifugated and resuspended in complete RPMI containing 11mM INO and no GLC. ADA-OE CAR-T cells were produced by co-transduction with CAR vector. As a surrogate for detection of overexpressed ADA, we used anti-HA.Tag antibody (BioLegend).

Clinical-grade GD2.bbz-CAR-T cell were manufactured using G-Rex (Wilson-Wolf). Apheresis of healthy donors was freshly collected and $CD4^+$/$CD8^+$ T cells were enriched using anti-CD4 and anti-CD8 beads (Miltenyi) and EasySep250 (StemCell). T cell activation was performed using Human T-Expander CD3/CD28 Dynabeads (Gibco) at a 1.5:1 bead:cell ratio at day 3. T cells were transduced with GD2 retrovector (MOI=10) on day 2 by spinning at 400g 32°C for 2hrs in the presence of 10μg/ml of protamine sulfate (Frezenius-Cabi). From day 3 to 7 cells were cultured in glucose- or inosine-containing complete RPMI. For small scale, T cells were activated using TransAct (Miltenyi). Day 3 post-activation, transact was washed off and cells were further cultured in TexMACS (Miltenyi) containing 3% human serum (ACCESS CELL CULTURE LLC) and 12.5ng/mL of IL-7 (Miltenyi) and IL-15 (Miltenyi).

CD39- cells were purified using anti-PE MicroBeads (Miltenyi) and LD autoMACS (Miltenyi Biotec) columns according to the manufacturer's protocol. Depletion efficiency was assessed by flow cytometry.

Flow cytometry—All flow analysis was performed at day 14/15 post-activation, unless differently indicated in the text. The anti-CD19-CAR idiotype antibody was provided by B. Jena and L.Cooper. The 1A7 anti-14G2a idiotype antibody was obtained from NCI Frederick and University of Texas M.D. Anderson Cancer Center. Her2.bbz-CAR was detected using BFP fluorescent protein integrated into the plasmid or human Her2-Fc recombinant proteins (R&D). The idiotype antibodies and Fc-fusion protein were conjugated with Dylight650 antibody labelling kits (Thermo Fisher).

Cell cycle was performed using APC BrDU kit (BD) according to the manufacturer protocol. Frequency of apoptotic cells was assessed using Annexin V Apoptosis Detection Kits (eBioscience) according to the manufacturer protocol.

Suppression assay—For assessing IL-2 secretion inhibition 5×10^4 CD19-BBz-CAR-T cells in the presence or absence of 5×10^4 of control, genetically modified bulk HA-CAR-T cells were cultured with 5×10^4 Nalm6 cells in 300μL CM in 96-well flat-bottom plates for 24h. $CD8^+$ HA-CAR-T cells were selected using anti-PE MicroBeads (Miltenyi) according to the manufacturer's protocol (average $CD8^+$ selection 90%). Triplicate wells were plated for each condition. Culture supernatants were collected and analyzed for IL-2 by ELISA (BioLegend).

Co-culture assays—HA- or CD19-BBz-CAR-T cells between day 14–16 post-activation were cultured with 10 or 40μM of CPI444 for 2 to 24 hours before the duration of coculture (unless stated otherwise) with tumor cells or plate-bound idiotype at the concentration 5μg/ml. To stimulate A2aR, cells were treated with 0.01–0.1mM of NECA. For cytotoxicity assays, approximately 5×10^4 of tumor cells were co-cultured with CAR-T cells at indicated ratio in 200μL CM in 96-well flat-bottom plates. Four images per well at 10x zoom were collected at each time point. Tumor growth was quantified by measuring total integrated GFP intensity per well using an IncuCyte ZOOM Live-Cell analysis system (Essen Bioscience) every 2–3hr. GFP signal was normalized to the time 0 signal. Supernatants were collected at 24 hours, and IL-2 and IFNγ were determined by ELISA. Triplicates were plated for each condition.

CRISPR knockout—CRISPR–Cas9 gene knockout was performed by transient Cas9/gRNA (RNP) complex electroporation using the P3 Primary Cell 4D-Nucleofector X Kit S (Lonza). On day 4 of culture, HA-CAR-T cells were counted, pelleted and resuspended in P3 buffer at 1.5×10^6–2×10^6 cells per 18μl reaction. 3.3μg Alt-R.Sp. Cas9 protein (IDT) and 120pmol chemically modified synthetic sgRNA (Synthego) (6:1 molar ratio gRNA:Cas9) per reaction was pre-complexed for 10min at RT to create ribonucleoprotein complexes (RNP). An 18μl cell suspension was mixed with RNP and electroporated using the EO-115 protocol in 16-well cuvette strips. Cells were recovered at 37°C for 30min in 200μl CM then expanded. Knockdown efficiency was determined using TIDE or flow cytometry if antibody was available. In the all experiments involving gene knockout, control CAR-T cells and ADA-OE cells were electroporated with a gRNA targeting the safe harbor locus AAVS1[68]. To increase purity of the knock out, $CD73^+$ cells were depleted using anti-PE MicroBeads (Miltenyi) according to the manufacturer's protocol.

Bulk RNAseq—On day 14, $CD39^+$ and $CD39^-$ $CD4^+$ or $CD8^+$ subsets were isolated using a BD FACSAria cell sorter (Stem Cell FACS Core, Stanford University School of Medicine). ADA-OE, CD39KO, CD73KO, A2aRKO and AAVS1KO HA-CAR-T cells were collected at day 15 post-activation. HA-CAR-T cells cultured in regular media or in the media containing INO but not GLC were collected at day 14. Total mRNA was isolated using Qiagen RNEasy Plus mini-isolation kit. Libraries and RNA-seq were performed by Novogene (Sacramento, CA) and 150 bp paired-end sequencing at a depth of 3×10^7 reads per sample was obtained using the Illumina NovaSeq6000 platform.

Reads mapping and counting were performed using STAR (version 2.7.6a) with GRCh38 as reference genome, HTSeq-count tools respectively. Genes having <10 counts in all samples in total were filtered out. PCA was performed using the scikit-learn package in python with default parameters on center-normalized transcript-per-million matrix. Differential gene expression analysis was performed using the DESeq2 package in R.

DAVID gene annotation enrichment analysis was performed using KEGG pathways and GO terms (biological process, cellular component, and molecular function). Functional annotation clustering was performed and terms with $p < 0.05$ (Benjamini corrected) are shown. Redundant terms were manually removed for visualization. Gene set enrichment

analysis was performed and the significant gene sets by P-value <0.05 and FDR <0.25 were visualized.

ATP measurements—CAR-T cells were washed with phenol-free RPMI (Agillent), next, 5×10^4 of cells were resuspended in 150μl phenol-free RPMI and spiked with 20μM ATP (PerkinElmer). After 10min of incubation at 37°C supernatants were collected and concentration of ATP/sample was measured using ATPlite Luminescence Assay System (PerkinElmer) according to the manufacturer's protocol.

ADO measurements—To measure the ability of ectoenzymes at the surface CAR-T cells were washed with phenol-free RPMI (Agillent). Next, 5×10^4 of cells were resuspended in 150μl phenol-free RPMI and spiked with 20μM ATP (PerkinElmer). After 30min of incubation at 37°C supernatants were collected. Ado concentration was assessed using Ado Assay Kit (abcam) according to the manufacturer's protocol.

Luminex—At day 14 post-activation sorted $CD39^+$ and $CD39^-$ $CD4^+$ or $CD8^+$ CAR-T cells were co cultured with Nalm6-GD2 at 1:1 ratio. Duplicates were plated for each condition. After 24hrs supernatants were collected and analyzed using Luminex assay performed at the Human Immune Monitoring Center of Stanford University. Human 62-plex kits were purchased from eBioscience/Affymetrix and used according to the manufacturer's recommendations with following modifications: beads were added to a 96-well plate and washed. Samples were added to the plate containing the mixed antibody-linked beads and incubated 1h RT followed by ON incubation at 4°C on an orbital shaker at 500–600rpm. Plates were washed biotinylated detection antibody was added for 75min at RT with shaking. The plate was washed and streptavidin-PE was added. After incubation for 30min at RT and washing, reading buffer was added to the wells. Plates were read using a Luminex FLEXMAP 3D instrument with a lower bound of 50 beads/sample/cytokine. Custom assay control beads by Radix Biosolutions were added to all wells. The dilution factor was accounted for. For each cytokine, concentration [pg/ml] was calculated.

QuantiBRITE antigen density quantification—The cell surface quantification of GD2 on tumor lines was enumerated by flow cytometry using BD QuantiBRITE beads and Custom Quantitation Beads (BD) according to the manufacturer's protocol.

Mass cytometry—1×10^6 cells were washed twice with PBS and resuspended in 1ml of PBS with 250nM cisplatin (Fluidigm).. Cells were incubated for 3min at RT and washed with cell staining medium (CSM, 1X PBS with 0.05% BSA, 0.02% sodium azide). Then cells were fixed with 1.6% paraformaldehyde in PBS for 10 min at RT, followed by a wash with 1X PBS. Samples were subsequently frozen using CryoStore (STEMCELL Technologies) for further use. Upon thawing and washing in CSM, barcoding was performed using a palladium-based approach using the Cell-ID 20-Plex Pd Barcoding Kit manufacturer's protocol (Fluidigm). Samples were mixed and treated as one for all subsequent steps. Titrated amounts of each cell surface antibody were mixed, filtered through a 0.1mm spin filter (Millipore), and added to the merged barcoded sample for 30min at room temperature. Cells were then washed twice with CSM and permeabilized by adding ice cold methanol for 10min at 4°C, followed by two washes with CSM. Finally,

samples were resuspended in IR-intercalator (0.5mM iridium intercalator and 1% PFA in 1X PBS), washed once with CSM and twice with ddH2O, and filtered through a 50mm cell strainer (Thermo Fisher). Sample was resuspended at 1×10^6 cells/ml in ddH2O with 1x EQ four-element beads (Fluidigm). Cells were acquired on a Fluidigm Helios mass cytometer.

Data was analyzed using OMIQ software.

Seahorse assay—Metabolic analysis was carried out using Seahorse Bioscience Analyzer XFe96. Briefly, 0.2×10^6 cells were resuspended in extracellular flux assay media supplemented with 11mM glucose, 2mM glutamine, and 1mM sodium pyruvate for Mito stress Test or 2mM glutamine only for Glycolytic Stress Test. Cells were plated on a Cell-Tak (Corning)–coated microplate. Mitochondrial activity and glycolytic parameters were measured by the oxygen consumption rate (OCR) (pmol/min) and extracellular acidification rate (ECAR) (mpH/min), respectively, with use of real-time injections of oligomycin (1.5μM), carbonyl cyanide ptrifluoromethoxyphenylhydrazone (0.5μM), and rotenone and antimycin (0.5μM each). A Glycolysis stress test was performed by adding D-Glucose (10 mM), oligomycin (2.5μM) and 2DG (50mM). All the parameters were calculated according to manufacturer's instructions (Seahorse Bioscience). Reagents were purchased from Agilent.

ATACseq—Approximately 100,000 CAR T cells were used per sample. Nuclei were isolated with ATAC-LB (10 mM Tris-HCl pH 7.4, 10 mM NaCl, 3 mM MgCl2, 0.1% IGEPAL) and used for tagmentation using Nextera DNA Library Preparation Kit (Illumina) from three donors. After tagmentation DNA was purified with MinElute PCR Purification Kit (Qiagen). Tagmented DNA was then amplified with Phusion high-fidelity PCR master mix (NEB) using 14 PCR cycles. Amplified libraries were purified again with MinElute PCR Purification Kit. Fragment distribution of libraries was assessed with Agilent Bioanalyzer and libraries were sequenced on the Illumina NovaSeq 6000 PE150 platform at a depth of 3×10^7 reads per sample. Sequencing was performed by Novogene (Sacramento, CA)

ATACSeq data analysis—The ENCODE ATAC-seq pipeline v2.0.3 was used for quality control and processing of ATAC-seq using default parameters. Briefly, raw ATAC-seq reads were trimmed with cutadapt to remove Illumina Nextera adapter sequences and aligned to hg19 using Bowtie2. Uniquely aligned reads were identified using picard MarkDuplicates with 73–85% non-duplicates mapped reads among all the samples. Peak from individual samples was called on Tn5-corrected insertion sites using MACS2. Reads from mitochondria and reads of low mapping quality (MAPQ<30) were excluded. A union peak set was compiled by extending peak summits to 500 bp, merging all summits, running bedtools cluster, selecting summits with the highest MACS2 score. Peaks intersecting with ENCODE hg19 blacklisted regions or regions on chrY and chrX were removed. For visualization, consensus peaks from biological replicates were merged and genome coverage plot was generated by IGV v1.9.0[69]. Only peaks with at least 5 counts-per-million in at least one of the samples were included in the downstream analyses. PCA was performed on the 5000 most variable peaks using the regularized log transform values from DESeq2 v1.30.1[70]. For differential peak accessibility analysis and transcription factor motif analysis

batch effects by donor were corrected with the function ComBat_seq from the sva package v3.38.0[71]. Transcription factor motif deviation analysis was carried out using chromVAR v1.12.0 as previously described[72] with human motifs from the JASPAR database. Motifs with significant differences (adjusted p-value <0.05) in deviations between in HA-INO and HA were ranked based on the size of the deviation difference. DESeq2 was used to identify peaks with significant (adjusted p-value <0.001) differential accessibility, of which two peak sets were established: one containing the 500 peaks with the strongest decrease and one with the 500 peaks with the strongest increase in accessibility in HA-INO vs HA. For these two peak sets relative motif enrichment was computed with HOMER's findMotifsGenome.pl using default parameters. The transcription factor motifs were ranked based on the p-values of the enrichment level.

Blood analysis—Blood was collected from the retro-orbital sinus into Microvette blood collection tubes with EDTA (Fisher Scientific). Whole blood was labeled with anti-CD45 (eBioscience). Next, red blood cells were lysed with FACS Lysing Solution (BD) according to manufacturer's instructions. Samples were mixed with CountBright Absolute Counting beads (ThermoFisher) before flow cytometry analysis.

QUANTIFICATION AND STATISTICAL ANALYSIS

Unless otherwise noted in the figure legends, statistical analyses for significant differences between groups were conducted using unpaired two-tailed t-tests without correction for multiple comparisons and without assuming consistent s.d. using GraphPad Prism 8.4. Significance for survival data was calculated using the log-rank Mantel–Cox test. Asterisks denoting statistical significance are in Graphpad Prism style with one, two, three, or four asterisks representing P values less than 0.05, 0.01, 0.001, and 0.0001, respectively. Graphical abstract and schematics were design in biorender.com.

Supplementary Material

Refer to Web version on PubMed Central for supplementary material.

Acknowledgments

This work was supported by the National Cancer Institute (5P30CA124435 and U54CA232568-01, C.L.M.), a sponsored research agreement with Lyell Immunopharma, the St. Baldrick's EPICC Team (Empowering Pediatric Immunotherapies for Childhood Cancer) (C.L.M.) and the Virginia and D.K. Ludwig Fund for Cancer Research (C.L.M.). C.L.M. is a member of the Parker Institute for Cancer Immunotherapy which supports the cancer immunotherapy program at Stanford. K.L.D is the Anne T. and Robert M. Bass Endowed Faculty Scholar in Pediatric Cancer and Blood Diseases. This work is supported by Stanford Maternal and Child Health Research Institute, R01 CA251858-01A1S1. A.T.S. is supported by Parker Institute for Cancer Immunology, Cancer Research Institute Lloyd J. Old STAR Award. S.M. is supported Parker Institute for Cancer Immunology. A.L. is supported by the Nuovo-Soldati Foundation and by ITMO Cancer AVIESAN (Alliance Nationale pour les Sciences de la Vie et de la Santé/National Alliance for the Life Sciences and Health) within the framework of the French Cancer Plan.

Declaration of interests

D.D.K, S.A.F., and C.L.M. are co-inventors on a pending patent application for inosine media supplementation during cell manufacturing. D.D.K and C.L.M. are inventors on a patent application for the use of T cells overexpressing ADA1/2 for cancer immunotherapy. C.L.M. holds equity in and receives research funding from Lyell Immunopharma, holds equity in and consults for Link Cell Therapies and C.L.M., and L.L. hold equity and consult for CARGO Therapeutics. L.L. and E.S. hold equity in Lyell Immunopharma. E.S consults for Lepton

Pharmaceuticals and Galaria. S.A.F. serves on the Scientific Advisory Boards for Alaunos Therapeutics and Fresh Wind Biotech and has equity interest in both; S.A.F. receives research funding from CARGO and Tune Therapeutics. S.P. is a current employee of and holds equity in CARGO. C.L.M. consults for Immatics, Mammoth, and Ensoma. A.T.S. is a cofounder of Immunai and Cartography Biosciences. A.T.S. receives research funding from Allogene Therapeutics and Merck Research Laboratories.

References

1. Vijayan D, Young A, Teng MWL, and Smyth MJ (2017). Targeting immunosuppressive adenosine in cancer. Nature Reviews Cancer. Nature Publishing Group.
2. Mandapathil M, Hilldorfer B, Szczepanski MJ, Czystowska M, Szajnik M, Ren J, Lang S, Jackson EK, Gorelik E, and Whiteside TL (2010). Generation and accumulation of immunosuppressive adenosine by human CD4+CD25highFOXP3+ regulatory T Cells. Journal of Biological Chemistry 285, 7176–7186. 10.1074/jbc.M109.047423. [PubMed: 19858205]
3. Jarvis LB, Rainbow DB, Coppard V, Howlett SK, Georgieva Z, Davies JL, Mullay HK, Hester J, Ashmore T, Bosch AVD, et al. (2021). Therapeutically expanded human regulatory T-cells are super-suppressive due to HIF1A induced expression of CD73. Commun. Biol 4, 1186. 10.1038/s42003-021-02721-x. [PubMed: 34650224]
4. Kudryavtsev I, Serebriakova M, Zhiduleva E, Murtazalieva P, Titov V, Malashicheva A, Shishkova A, Semenova D, Irtyuga O, Isakov D, et al. (2019). CD73 Rather Than CD39 Is Mainly Involved in Controlling Purinergic Signaling in Calcified Aortic Valve Disease. Front. Genet 10, 604. 10.3389/fgene.2019.00604. [PubMed: 31402927]
5. Sims S, Colston J, Bolinger B, Emery V, and Klenerman P (2014). CD73 Is Dispensable for the Regulation of Inflationary CD8+ T-Cells after Murine Cytomegalovirus Infection and Adenovirus Immunisation. PLoS ONE 9, e114323. 10.1371/journal.pone.0114323. [PubMed: 25490556]
6. Simoni Y, Becht E, Fehlings M, Loh CY, Koo S-L, Teng KWW, Yeong JPS, Nahar R, Zhang T, Kared H, et al. (2018). Bystander CD8+ T cells are abundant and phenotypically distinct in human tumour infiltrates. Nature 557, 575–579. 10.1038/s41586-018-0130-2. [PubMed: 29769722]
7. Duhen T, Duhen R, Montler R, Moses J, Moudgil T, de Miranda NF, Goodall CP, Blair TC, Fox BA, McDermott JE, et al. (2018). Co-expression of CD39 and CD103 identifies tumor-reactive CD8 T cells in human solid tumors. Nat Commun 9, 2724. 10.1038/s41467-018-05072-0. [PubMed: 30006565]
8. Kortekaas KE, Santegoets SJ, Sturm G, Ehsan I, van Egmond SL, Finotello F, Trajanoski Z, Welters MJP, van Poelgeest MIE, and van der Burg SH (2020). CD39 Identifies the CD4(+) Tumor-Specific T-cell Population in Human Cancer. Cancer Immunol Res 8, 1311–1321. 10.1158/2326-6066.CIR-20-0270. [PubMed: 32759363]
9. Eiva MA, Omran DK, Chacon JA, and Powell DJ Jr. (2022). Systematic analysis of CD39, CD103, CD137, and PD-1 as biomarkers for naturally occurring tumor antigen-specific TILs. Eur J Immunol 52, 96–108. 10.1002/eji.202149329. [PubMed: 34505280]
10. Liu T, Tan J, Wu M, Fan W, Wei J, Zhu B, Guo J, Wang S, Zhou P, Zhang H, et al. (2021). High-affinity neoantigens correlate with better prognosis and trigger potent antihepatocellular carcinoma (HCC) activity by activating CD39+CD8+ T cells. Gut 70, 1965–1977. 10.1136/gutjnl-2020-322196. [PubMed: 33262196]
11. Luo Y, Zong Y, Hua H, Gong M, Peng Q, Li C, Neculai D, and Zeng X (2022). Immune-infiltrating signature-based classification reveals CD103+CD39+ T cells associate with colorectal cancer prognosis and response to immunotherapy. Front. Immunol 13, 1011590. 10.3389/fimmu.2022.1011590. [PubMed: 36311750]
12. Qi Y, Xia Y, Lin Z, Qu Y, Qi Y, Chen Y, Zhou Q, Zeng H, Wang J, Chang Y, et al. (2020). Tumor-infiltrating CD39+CD8+ T cells determine poor prognosis and immune evasion in clear cell renal cell carcinoma patients. Cancer Immunol., Immunother 69, 1565–1576. 10.1007/s00262-020-02563-2. [PubMed: 32306075]
13. Canale FP, Ramello MC, Núñez N, Furlan CLA, Bossio SN, Serrán MG, Boari JT, Del Castillo A, Ledesma M, Sedlik C, et al. (2018). CD39 expression defines cell exhaustion in tumor-infiltrating CD8+ T cells. Cancer Research 78, 115–128. 10.1158/0008-5472.CAN-16-2684. [PubMed: 29066514]

14. Weber EW, Parker KR, Sotillo E, Lynn RC, Anbunathan H, Lattin J, Good Z, Belk JA, Daniel B, Klysz D, et al. (2021). Transient rest restores functionality in exhausted CAR-T cells through epigenetic remodeling. Science 372. 10.1126/science.aba1786.

15. Krishna S, Lowery FJ, Copeland AR, Bahadiroglu E, Mukherjee R, Jia L, Anibal JT, Sachs A, Adebola SO, Gurusamy D, et al. (2020). Stem-like CD8 T cells mediate response of adoptive cell immunotherapy against human cancer. Science 370, 1328–1334. 10.1126/science.abb9847. [PubMed: 33303615]

16. Weber EW, Maus MV, and Mackall CL (2020). The Emerging Landscape of Immune Cell Therapies. Cell Cell Press.

17. Long AH, Haso WM, Shern JF, Wanhainen KM, Murgai M, Ingaramo M, Smith JP, Walker AJ, Kohler ME, Venkateshwara VR, et al. (2015). 4–1BB costimulation ameliorates T cell exhaustion induced by tonic signaling of chimeric antigen receptors. Nat Med 21, 581–590. 10.1038/nm.3838. [PubMed: 25939063]

18. Deng Q, Han G, Puebla-Osorio N, Ma MCJ, Strati P, Chasen B, Dai E, Dang M, Jain N, Yang H, et al. (2020). Characteristics of anti-CD19 CAR T cell infusion products associated with efficacy and toxicity in patients with large B cell lymphomas. Nature Medicine 26, 1878–1887. 10.1038/s41591-020-1061-7.

19. Wang M, Munoz J, Goy A, Locke FL, Jacobson CA, Hill BT, Timmerman JM, Holmes H, Jaglowski S, Flinn IW, et al. (2020). KTE-X19 CAR T-Cell Therapy in Relapsed or Refractory Mantle-Cell Lymphoma. New England Journal of Medicine 382, 1331–1342. 10.1056/nejmoa1914347. [PubMed: 32242358]

20. Locke FL, Ghobadi A, Jacobson CA, Miklos DB, Lekakis LJ, Oluwole OO, Lin Y, Braunschweig I, Hill BT, Timmerman JM, et al. (2019). Long-term safety and activity of axicabtagene ciloleucel in refractory large B-cell lymphoma (ZUMA-1): a single-arm, multicentre, phase 1–2 trial. The Lancet Oncology 20, 31–42. 10.1016/S1470-2045(18)30864-7. [PubMed: 30518502]

21. O'Rourke DM, Nasrallah MP, Desai A, Melenhorst JJ, Mansfield K, Morrissette JJD, Martinez-Lage M, Brem S, Maloney E, Shen A, et al. (2017). A single dose of peripherally infused EGFRvIII-directed CAR T cells mediates antigen loss and induces adaptive resistance in patients with recurrent glioblastoma. Science Translational Medicine 9. 10.1126/scitranslmed.aaa0984.

22. Shi D, Shi Y, Kaseb AO, Qi X, Zhang Y, Chi J, Lu Q, Gao H, Jiang H, Wang H, et al. (2020). Chimeric Antigen Receptor-Glypican-3 T-Cell Therapy for Advanced Hepatocellular Carcinoma: Results of Phase I Trials. Clinical Cancer Research 26, 3979–3989. 10.1158/1078-0432.CCR-19-3259. [PubMed: 32371538]

23. Majzner RG, Ramakrishna S, Yeom KW, Patel S, Chinnasamy H, Schultz LM, Richards RM, Jiang L, Barsan V, Mancusi R, et al. (2022). GD2-CAR T cell therapy for H3K27M-mutated diffuse midline gliomas. Nature 603, 934–941. 10.1038/s41586-022-04489-4. [PubMed: 35130560]

24. Lynn RC, Weber EW, Sotillo E, Gennert D, Xu P, Good Z, Anbunathan H, Lattin J, Jones R, Tieu V, et al. (2019). c-Jun overexpression in CAR T cells induces exhaustion resistance. Nature 576, 293–300. 10.1038/s41586-019-1805-z. [PubMed: 31802004]

25. Mascanfroni ID, Yeste A, Vieira SM, Burns EJ, Patel B, Sloma I, Wu Y, Mayo L, Ben-Hamo R, Efroni S, et al. (2013). IL-27 acts on DCs to suppress the T cell response and autoimmunity by inducing expression of the immunoregulatory molecule CD39. Nat Immunol 14, 1054–1063. 10.1038/ni.2695. [PubMed: 23995234]

26. Do JS, Visperas A, Sanogo YO, Bechtel JJ, Dvorina N, Kim S, Jang E, Stohlman SA, Shen B, Fairchild RL, et al. (2016). An IL-27/Lag3 axis enhances Foxp3+ regulatory T cell-suppressive function and therapeutic efficacy. Mucosal Immunology 9, 137–145. 10.1038/mi.2015.45. [PubMed: 26013006]

27. Batlle E, and Massagué J (2019). Transforming Growth Factor-β Signaling in Immunity and Cancer. Immunity Cell Press.

28. Chen J, López-Moyado IF, Seo H, Lio CWJ, Hempleman LJ, Sekiya T, Yoshimura A, Scott-Browne JP, and Rao A (2019). NR4A transcription factors limit CAR T cell function in solid tumours. Nature 567, 530–534. 10.1038/s41586-019-0985-x. [PubMed: 30814732]

29. Takeuchi H, Yokota-Nakatsuma A, Ohoka Y, Kagechika H, Kato C, Song S-Y, and Iwata M (2013). Retinoid X Receptor Agonists Modulate Foxp3 + Regulatory T Cell and Th17 Cell

Differentiation with Differential Dependence on Retinoic Acid Receptor Activation. J. Immunol 191, 3725–3733. 10.4049/jimmunol.1300032. [PubMed: 23980207]

30. Good CR, Aznar MA, Kuramitsu S, Samareh P, Agarwal S, Donahue G, Ishiyama K, Wellhausen N, Rennels AK, Ma Y, et al. (2021). An NK-like CAR T cell transition in CAR T cell dysfunction. Cell 184, 6081–6100 e6026. 10.1016/j.cell.2021.11.016. [PubMed: 34861191]
31. Weber EW, Lynn RC, Sotillo E, Lattin J, Xu P, and Mackall CL (2019). Pharmacologic control of CAR-T cell function using dasatinib. Blood Advances 3, 711–717. 10.1182/bloodadvances.2018028720. [PubMed: 30814055]
32. Peres RS, Donate PB, Talbot J, Cecilio NT, Lobo PR, Machado CC, Lima KWA, Oliveira RD, Carregaro V, Nakaya HI, et al. (2018). TGF-β signalling defect is linked to low CD39 expression on regulatory T cells and methotrexate resistance in rheumatoid arthritis. Journal of Autoimmunity 90, 49–58. 10.1016/j.jaut.2018.01.004. [PubMed: 29426578]
33. Deaglio S, Dwyer KM, Gao W, Friedman D, Usheva A, Erat A, Chen JF, Enjyoji K, Linden J, Oukka M, et al. (2007). Adenosine generation catalyzed by CD39 and CD73 expressed on regulatory T cells mediates immune suppression. Journal of Experimental Medicine 204, 1257–1265. 10.1084/jem.20062512. [PubMed: 17502665]
34. Leone RD, Sun IM, Oh MH, Sun IH, Wen J, Englert J, and Powell JD (2018). Inhibition of the adenosine A2a receptor modulates expression of T cell coinhibitory receptors and improves effector function for enhanced checkpoint blockade and ACT in murine cancer models. Cancer Immunol., Immunother 67, 1271–1284. 10.1007/s00262-018-2186-0. [PubMed: 29923026]
35. Fraietta JA, Lacey SF, Orlando EJ, Pruteanu-Malinici I, Gohil M, Lundh S, Boesteanu AC, Wang Y, O'Connor RS, Hwang WT, et al. (2018). Determinants of response and resistance to CD19 chimeric antigen receptor (CAR) T cell therapy of chronic lymphocytic leukemia. Nature Medicine 24, 563–571. 10.1038/s41591-018-0010-1.
36. Van Gassen S, Callebaut B, Van Helden MJ, Lambrecht BN, Demeester P, Dhaene T, and Saeys Y (2015). FlowSOM: Using self-organizing maps for visualization and interpretation of cytometry data. Cytometry Part A 87, 636–645. 10.1002/cyto.a.22625.
37. Utzschneider DT, Gabriel SS, Chisanga D, Gloury R, Gubser PM, Vasanthakumar A, Shi W, and Kallies A (2020). Early precursor T cells establish and propagate T cell exhaustion in chronic infection. Nat Immunol 21, 1256–1266. 10.1038/s41590-020-0760-z. [PubMed: 32839610]
38. Guo Y, Xie Y-Q, Gao M, Zhao Y, Franco F, Wenes M, Siddiqui I, Bevilacqua A, Wang H, Yang H, et al. (2021). Metabolic reprogramming of terminally exhausted CD8+ T cells by IL-10 enhances anti-tumor immunity. Nat Immunol 22, 746–756. 10.1038/s41590-021-00940-2. [PubMed: 34031618]
39. Wang T, Gnanaprakasam JNR, Chen X, Kang S, Xu X, Sun H, Liu L, Rodgers H, Miller E, Cassel TA, et al. (2020). Inosine is an alternative carbon source for CD8+− T-cell function under glucose restriction. Nature Metabolism 2, 635–647. 10.1038/s42255-020-0219-4.
40. Majzner RG, Rietberg SP, Sotillo E, Dong R, Vachharajani VT, Labanieh L, Myklebust JH, Kadapakkam M, Weber EW, Tousley AM, et al. (2020). Tuning the Antigen Density Requirement for CAR T-cell Activity. Cancer Discov 10, 702–723. 10.1158/2159-8290.CD-19-0945. [PubMed: 32193224]
41. Klein Geltink RI, Edwards-Hicks J, Apostolova P, O'Sullivan D, Sanin DE, Patterson AE, Puleston DJ, Ligthart NAM, Buescher JM, Grzes KM, et al. (2020). Metabolic conditioning of CD8(+) effector T cells for adoptive cell therapy. Nat Metab 2, 703–716. 10.1038/s42255-020-0256-z. [PubMed: 32747793]
42. Kinjyo I, Qin J, Tan S-Y, Wellard CJ, Mrass P, Ritchie W, Doi A, Cavanagh LL, Tomura M, Sakaue-Sawano A, et al. (2015). Real-time tracking of cell cycle progression during CD8+ effector and memory T-cell differentiation. Nat Commun 6, 6301. 10.1038/ncomms7301. [PubMed: 25709008]
43. Chapman NM, and Chi H (2018). Hallmarks of T-cell Exit from Quiescence. Cancer Immunol Res 6, 502–508. 10.1158/2326-6066.cir-17-0605. [PubMed: 29716982]
44. Giuffrida L, Sek K, Henderson MA, Lai J, Chen AXY, Meyran D, Todd KL, Petley EV, Mardiana S, Mølck C, et al. (2021). CRISPR/Cas9 mediated deletion of the adenosine A2A receptor enhances CAR T cell efficacy. Nat Commun 12. 10.1038/s41467-021-23331-5.

45. Hartmann FJ, Mrdjen D, McCaffrey E, Glass DR, Greenwald NF, Bharadwaj A, Khair Z, Verberk SGS, Baranski A, Baskar R, et al. (2021). Single-cell metabolic profiling of human cytotoxic T cells. Nat Biotechnol 39, 186–197. 10.1038/s41587-020-0651-8. [PubMed: 32868913]
46. Verrey F, Closs EI, Wagner CA, Palacin M, Endou H, and Kanai Y (2004). CATs and HATs: the SLC7 family of amino acid transporters. Pflügers Archiv 447, 532–542. 10.1007/s00424-003-1086-z. [PubMed: 14770310]
47. Puleston DJ, Baixauli F, Sanin DE, Edwards-Hicks J, Villa M, Kabat AM, Kamiński MM, Stanckzak M, Weiss HJ, Grzes KM, et al. (2021). Polyamine metabolism is a central determinant of helper T cell lineage fidelity. Cell 184, 4186–4202.e4120. 10.1016/j.cell.2021.06.007. [PubMed: 34216540]
48. Yerinde C, Siegmund B, Glauben R, and Weidinger C (2019). Metabolic Control of Epigenetics and Its Role in CD8+ T Cell Differentiation and Function. Front. Immunol Frontiers Media S.A.
49. Gennert DG, Lynn RC, Granja JM, Weber EW, Mumbach MR, Zhao Y, Duren Z, Sotillo E, Greenleaf WJ, Wong WH, et al. (2021). Dynamic chromatin regulatory landscape of human CAR T cell exhaustion. Proc Natl Acad Sci U S A 118. 10.1073/pnas.2104758118.
50. Milner JJ, Toma C, Yu B, Zhang K, Omilusik K, Phan AT, Wang D, Getzler AJ, Nguyen T, Crotty S, et al. (2017). Runx3 programs CD8+ T cell residency in non-lymphoid tissues and tumours. Nature 552, 253–257. 10.1038/nature24993. [PubMed: 29211713]
51. Tan TCJ, Kelly V, Zou X, Wright D, Ly T, and Zamoyska R (2022). Translation factor eIF5a is essential for IFNγ production and cell cycle regulation in primary CD8+ T lymphocytes. Nat Commun 13, 7796. 10.1038/s41467-022-35252-y. [PubMed: 36528626]
52. Bausch-Fluck D, Goldmann U, Muller S, van Oostrum M, Muller M, Schubert OT, and Wollscheid B (2018). The in silico human surfaceome. Proc Natl Acad Sci U S A 115, E10988–E10997. 10.1073/pnas.1808790115. [PubMed: 30373828]
53. Allard B, Allard D, Buisseret L, and Stagg J (2020). The adenosine pathway in immuno-oncology. Nat Rev Clin Oncol 17, 611–629. 10.1038/s41571-020-0382-2. [PubMed: 32514148]
54. Vignali PDA, DePeaux K, Watson MJ, Ye C, Ford BR, Lontos K, McGaa NK, Scharping NE, Menk AV, Robson SC, et al. (2023). Hypoxia drives CD39-dependent suppressor function in exhausted T cells to limit antitumor immunity. Nat Immunol 24, 267–279. 10.1038/s41590-022-01379-9. [PubMed: 36543958]
55. Qu Y, Dunn ZS, Chen X, MacMullan M, Cinay G, Wang HY, Liu J, Hu F, and Wang P (2022). Adenosine Deaminase 1 Overexpression Enhances the Antitumor Efficacy of Chimeric Antigen Receptor-Engineered T Cells. Hum Gene Ther 33, 223–236. 10.1089/hum.2021.050. [PubMed: 34225478]
56. Dolce LG, Zimmer AA, Tengo L, Weis F, Rubio MAT, Alfonzo JD, and Kowalinski E (2022). Structural basis for sequence-independent substrate selection by eukaryotic wobble base tRNA deaminase ADAT2/3. Nat Commun 13, 6737. 10.1038/s41467-022-34441-z. [PubMed: 36347890]
57. Mager LF, Burkhard R, Pett N, Cooke NCA, Brown K, Ramay H, Paik S, Stagg J, Groves RA, Gallo M, et al. (2020). Microbiome-derived inosine modulates response to checkpoint inhibitor immunotherapy https://www.science.org.
58. Saveljeva S, Sewell GW, Ramshorn K, Cader MZ, West JA, Clare S, Haag LM, de Almeida Rodrigues RP, Unger LW, Iglesias-Romero AB, et al. (2022). A purine metabolic checkpoint that prevents autoimmunity and autoinflammation. Cell Metab 34, 106–124 e110. 10.1016/j.cmet.2021.12.009. [PubMed: 34986329]
59. Boswell-Casteel RC, and Hays FA (2017). Equilibrative nucleoside transporters—A review. Nucleosides, Nucleotides Nucleic Acids 36, 7–30. 10.1080/15257770.2016.1210805.
60. Bao R, Hou J, Li Y, Bian J, Deng X, Zhu X, and Yang T (2016). Adenosine promotes Foxp3 expression in Treg cells in sepsis model by activating JNK/AP-1 pathway. Am. J. Transl. Res 8, 2284–2292. [PubMed: 27347335]
61. Klysz D, Tai X, Robert PA, Craveiro M, Cretenet G, Oburoglu L, Mongellaz C, Floess S, Fritz V, Matias MI, et al. (2015). Glutamine-dependent α-ketoglutarate production regulates the balance between T helper 1 cell and regulatory T cell generation. Science Signaling 8. 10.1126/scisignal.aab2610.

62. Zhao S, Peralta RM, Avina-Ochoa N, Delgoffe GM, and Kaech SM (2021). Metabolic regulation of T cells in the tumor microenvironment by nutrient availability and diet. Semin Immunol 52, 101485. 10.1016/j.smim.2021.101485. [PubMed: 34462190]

63. Fox CJ, Hammerman PS, and Thompson CB (2005). Fuel feeds function: energy metabolism and the T-cell response. Nat Rev Immunol 5, 844–852. 10.1038/nri1710. [PubMed: 16239903]

64. O'Sullivan D, vanderWindt GWJ, Huang SCC, Curtis JD, Chang CH, Buck MDL, Qiu J, Smith AM, Lam WY, DiPlato LM, et al. (2014). Memory CD8+ T Cells Use Cell-Intrinsic Lipolysis to Support the Metabolic Programming Necessary for Development. Immunity 41, 75–88. 10.1016/j.immuni.2014.06.005. [PubMed: 25001241]

65. Wang R, Dillon CP, Shi LZ, Milasta S, Carter R, Finkelstein D, McCormick LL, Fitzgerald P, Chi H, Munger J, and Green DR (2011). The Transcription Factor Myc Controls Metabolic Reprogramming upon T Lymphocyte Activation. Immunity 35, 871–882. 10.1016/j.immuni.2011.09.021. [PubMed: 22195744]

66. Puleston DJ, Buck MD, Klein Geltink RI, Kyle RL, Caputa G, O'Sullivan D, Cameron AM, Castoldi A, Musa Y, Kabat AM, et al. (2019). Polyamines and eIF5A Hypusination Modulate Mitochondrial Respiration and Macrophage Activation. Cell Metabolism 30, 352–363.e358. 10.1016/j.cmet.2019.05.003. [PubMed: 31130465]

67. Ghassemi S, Durgin JS, Nunez-Cruz S, Patel J, Leferovich J, Pinzone M, Shen F, Cummins KD, Plesa G, Cantu VA, et al. (2022). Rapid manufacturing of non-activated potent CAR T cells. Nat Biomed Eng 6, 118–128. 10.1038/s41551-021-00842-6. [PubMed: 35190680]

68. Ogata T, Kozuka T, and Kanda T (2003). Identification of an Insulator in AAVS1, a Preferred Region for Integration of Adeno-Associated Virus DNA. J Virol 77, 9000–9007. 10.1128/jvi.77.16.9000-9007.2003. [PubMed: 12885916]

69. Robinson JT, Thorvaldsdóttir H, Winckler W, Guttman M, Lander ES, Getz G, and Mesirov JP (2011). Integrative genomics viewer. Nat Biotechnol 29, 24–26. 10.1038/nbt.1754. [PubMed: 21221095]

70. Love MI, Huber W, and Anders S (2014). Moderated estimation of fold change and dispersion for RNA-seq data with DESeq2. Genome Biol 15, 550. 10.1186/s13059-014-0550-8. [PubMed: 25516281]

71. Zhang Y, Parmigiani G, and Johnson WE (2020). ComBat-seq: batch effect adjustment for RNA-seq count data. NAR Genom Bioinform 2, lqaa078. 10.1093/nargab/lqaa078. [PubMed: 33015620]

72. Schep AN, Wu B, Buenrostro JD, and Greenleaf WJ (2017). chromVAR: inferring transcription-factor-associated accessibility from single-cell epigenomic data. Nat Methods 14, 975–978. 10.1038/nmeth.4401. [PubMed: 28825706]

Highlights

- Exhausted CAR-T cells generate immunosuppressive adenosine through CD39/CD73
- Increased inosine metabolism induces stemness
- CAR-T cells cultured in inosine-containing media have increased effector function
- Inosine supplementation is a novel strategy to improve CAR-T cell manufacturing

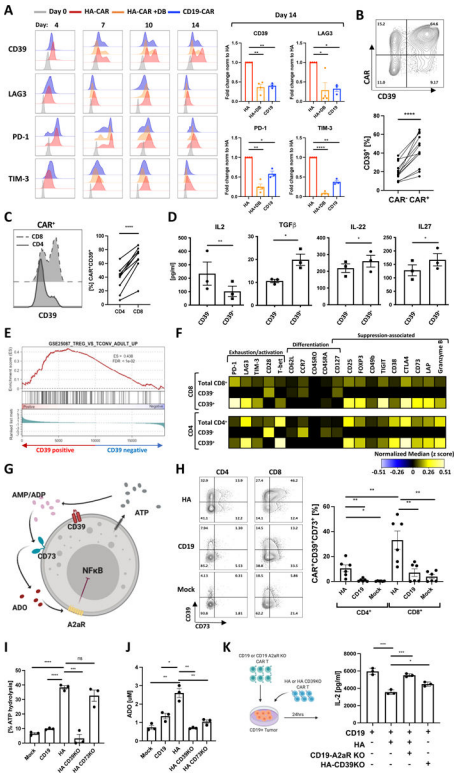

Figure 1: CD39 marks a subset of exhausted CAR T cells with features of regulatory T cells.

A. (Left) Flow cytometric analysis of exhaustion marker expression in gated CD19.28z-CAR$^+$ (CD19) (blue), HA.28z-CAR$^+$ (HA) (red) or treated starting D4 with dasatinib (HA+DB) (orange) T cells at D0 (grey) and at each indicated time-point post-activation. Representative histogram shown of n = 3–4 donors. (Right) Corresponding frequencies of exhaustion markers at D14 post-activation. Pooled data from n=3–4 donors.

B. (Top) Representative flow cytometry contour plot of CD39 expression in HA-CAR$^-$ vs. CAR$^+$-T cells on day 10 post-activation. (Bottom) Percent of CD39$^+$ cells in HA-CAR$^-$ vs. CAR$^+$-T cells (n=12 donors).

C. (Left) Representative flow cytometry analysis of CD39 expression in CD8$^+$ vs. CD4$^+$ HA-CAR-T cells 10 days post-activation. (Right) Percent of CD39$^+$ cells in CD4$^+$ vs. CD8$^+$ HA-CAR-T cells from n=9 donors.

D. Luminex analysis of cytokines secreted by CD39$^+$ vs. CD39$^-$CD8$^+$ HA-CAR-T cells sorted on day 14 and stimulated with Nalm6-GD2 for 24hrs at 1:1 E:T ratio. Data are mean ± s.e.m. of n=3 donors.

E. Gene Set Enrichment Analysis (GSEA) of bulk RNA-seq collected 14 days post-activation of CD39$^+$compared to CD39$^-$HA-CAR-T cells using the publicly available GSE25087 gene collection.

F. CyTOF analysis of CD4$^+$ (bottom) and CD8$^+$ (top) HA-CAR-T cells gated based on CD39 expression 10 days post-activation. Heat map represents expression of the indicated markers as median Arcsinh relative to the total CD4$^+$ or CD8$^+$ sample. Representative donor shown of n=3 donors.

G. Schematic of immune suppression mediated by purinergic pathway. ATP- adenosine triphosphate; ADP- adenosine diphosphate; AMP- adenosine monophosphate; ADO-

adenosine (red); A2aR- adenosine 2a receptor; CD39- ecto-ATP diphosphohydrolase-1; CD73- 5′-ectonucleotidase; NF-κB- Nuclear Factor kappa B.

H. (Left) Representative flow cytometry contour plots showing expression of CD39 and CD73 in gated $CD4^+$ or $CD8^+$ HA-, CD19-CAR- or mock T cells 14 days post-activation. (Right) Percent of $CD39^+CD73^+$ T cells in $CD4^+$ vs. $CD8^+$ by day 14 HA-, CD19-CAR or mock T cells in 6 donors.

I. Percent of ATP hydrolyzed by mock or CAR-expressing T cells with or without CD39 or CD73 after spiking with 20μM of ATP at day 15 post-activation. Representative data from n=4 donors. Average purity of the knock-out cells was > 90%. P values determined by unpaired two-tailed t-tests.

J. Concentration of adenosine (ADO) produced by mock or CAR-expressing T cells with or without CD39 or CD73 spiked with 20μM of ATP at day 17 post-activation. Representative data from n=3–5 donors. Average purity of the knock-out cells was > 90%. P values determined by unpaired two-tailed t-tests.

K. (Left) schematic of experimental design of immunosuppression co-culture assays. (Right) Control or A2aR KO CD19.bbz-CAR-T cells were activated with Nalm6 at 1:1 ratio in the presence of HA- or CD39KO HA-CAR-T cells. IL-2 was measured 24hrs post-stimulation. Data are mean ± s.e.m. from triplicate wells. P values determined by unpaired two-tailed t-tests. Representative result of two independent experiments.

P values determined by paired two-tailed t-tests unless otherwise specified. *, $P < 0.05$; **, $P < 0.01$; ***, $P < 0.001$; ****, $P < 0.0001$

See also Figure S1.

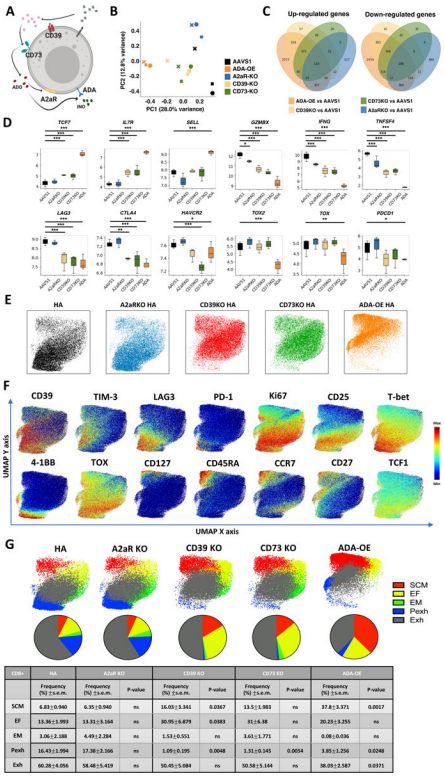

CD8+	HA	A2aR KO		CD39 KO		CD73 KO		ADA-OE	
	Frequency (%) ± s.e.m.	Frequency (%) ± s.e.m.	P-value	Frequency (%) ± s.e.m.	P-value	Frequency (%) ± s.e.m.	P-value	Frequency (%) ± s.e.m.	P-value
SCM	6.83 ± 0.940	6.35 ± 0.940	ns	16.03 ± 3.341	0.0367	13.5 ± 1.983	ns	37.8 ± 3.371	0.0017
EF	13.36 ± 1.993	13.31 ± 3.164	ns	30.95 ± 6.879	0.0383	31 ± 6.38	ns	20.23 ± 3.255	ns
EM	3.06 ± 2.188	4.49 ± 2.284	ns	1.53 ± 0.551	ns	3.61 ± 1.771	ns	0.08 ± 0.036	ns
Pexh	10.43 ± 1.994	17.38 ± 2.166	ns	1.09 ± 0.195	0.0048	1.31 ± 0.145	0.0054	3.85 ± 1.256	0.0248
Exh	66.28 ± 4.056	58.48 ± 5.419	ns	50.45 ± 5.084	ns	50.58 ± 5.144	ns	38.09 ± 2.587	0.0371

Figure 2: Overexpression of Adenosine deaminase (ADA-OE) increases features of stemness and decreases terminal differentiation.

A. Schematic of immune suppression mediated by purinergic pathway. ADO- adenosine (red); A2aR- adenosine 2a receptor; CD39- ecto-ATP diphosphohydrolase-1; CD73- 5′-ectonucleotidase; INO- inosine (green); ADA- adenosine deaminase.

B. Principal component analysis (PCA) of bulk RNA-seq from control AAVS1KO HA-CAR-T cells or overexpressing Ado deaminase (ADA-OE) or deficient for A2aR, CD39 or CD73 15 days post-activation (n=3 donors).

C. Number of up-regulated and down-regulated genes in ADA-OE, CD39-KO, CD73-KO and A2aR-KO conditions compared to AAVS1 controls.

D. Boxplots showing log2TPM of T cell exhaustion and effector associated genes in CAR T cells profiled by bulk RNA-seq. The top, bottom, middle and whiskers of the boxplot represents the upper quantile, lower quantile, median and the rest of the distribution, respectively *, $P < 0.1$; ** $P < 0.05$; *** $P < 0.01$ by DESeq2.

E-G. UMAP analysis of day 15 $CD8^+$ HA-CAR cells engineered as in (A). Expression of 26 markers was analyzed by CyTOF. 5,000 or maximum of $CD8^+$ CAR-T cells from each donor (n=4) were combined and colored by (E) genotype, (F) marker intensity or (G) subpopulation defined by FlowSOM algorithm. Pie charts show population frequencies defined using FlowSOM for each condition. SCM; stem cell memory, EF; effector, EM; effector memory, Pexh; progenitor exhausted, Exh, exhausted. Table shows the average frequencies and corresponding p values determined by paired two-tailed t-tests.

See also Figure S2.

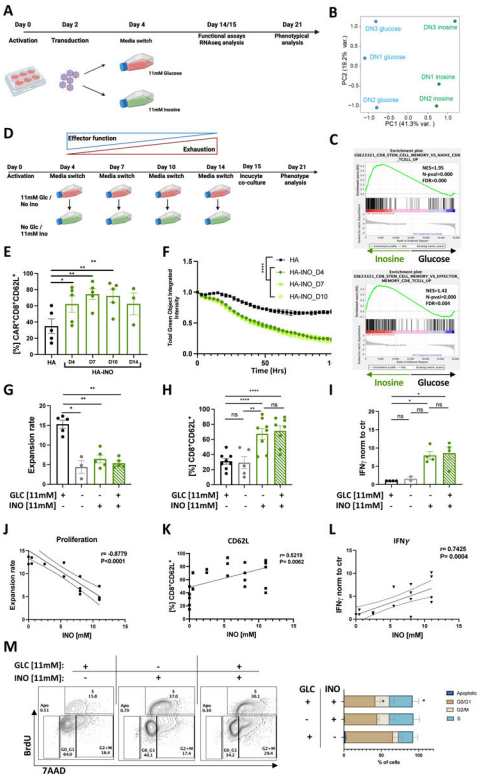

Figure 3: Inosine (INO) induces stemness and augments CAR T cell function in vitro.

A. Schematic of the experimental design.

B. PCA of bulk RNA-seq from HA-CAR-T cells expanded in indicated media for 10 days.

C. GSEA of HA-CAR-T cells expanded as in (B) using the GSE23321 gene collection.

D. Schematic of the experimental design.

E. Frequency of $CD8^{+}CD62L^{+}$ HA-CAR-T cells cultured in INO-media starting from the indicated days and assessed by flow cytometry at day 21 (n=5 donors).

F. Co-cultures of HA, or HA-CAR-T cells grown in INO media starting from indicated days post-activation and 143B tumor (1:1 E:T) starting at day 15 post-activation. Tumor GFP fluorescence intensity was normalized to the first time point (duplicate or triplicate wells). Representative donor of n=3 donor shown. P values determined by two-way ANOVA with Dunnett's multiple comparisons test.

G. Cell expansion of HA-CAR-T cells grown in culture media containing indicated concentration of glucose and/or inosine from day 4 to 10 post-activation. Data are mean ± s.e.m. of n=3–5 donors.

H. Percent of $CD62L^{+}CD8^{+}$ HA-CAR-T cells grown in culture media containing indicated concentration of glucose and/or inosine from day 4 to 21 and measured by flow cytometry. Data are mean ± s.e.m. of n=5–8 donors.

I. Fold increase of IFNγ release after 24hrs of co-culture with Nalm6-GD2 by D14 HA-CAR-T cells grown in culture media containing various concentrations of glucose and/or inosine and normalized to CAR-T cells grown in control media. Data are mean ± s.e.m. of n=2–4 donors.

J. Expansion of HA-CAR-T cells grown in RPMI containing 11mM of glucose and increasing concentrations of inosine for 6 days. Scatter plot showing correlation between

ratio of expansion (y-axis) and inosine concentration (x-axis). Pearson correlation, r, n=2–4 donors from independent experiments.

K. HA-CAR-T cells were grown in RPMI containing 11mM of glucose and increasing concentrations of inosine for 17 days. Scatter plot showing correlation between CD62L frequency (y-axis) and inosine concentration (x-axis). Pearson correlation, r, n=2–6 donors from independent experiments.

L. HA-CAR-T cells were grown in RPMI containing 11mM of glucose and increasing concentrations of inosine for 10 days, and stimulated with Nalm6-GD2 for 24hrs. Scatter plot showing correlation between IFNγ secretion (y-axis) and inosine concentration (x-axis). Pearson correlation, r, n=2–4 donors from independent experiments.

M. At day 10 post-activation HA-CAR-T cells were collected and cell cycle state was evaluated using BrdU and 7AAD staining. (Left) representative dot plots shown from one donor (n=3). (Right) Bar graphs represent percentage of apoptotic cells or in G0/G1, S and G2/M phase indicated for each media conditions. Data are mean+/− s.e.m. from n=3 donors. P values determined by paired two-tailed t-tests unless otherwise specified. *, $P < 0.05$; **, $P < 0.01$; ***, $P < 0.001$; ****, $P < 0.0001$

See also Figures S3 and S4.

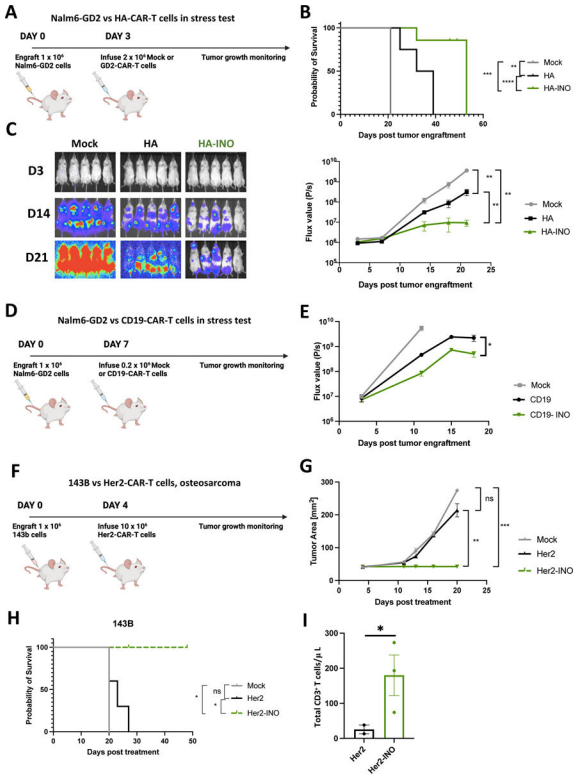

Figure 4: Inosine enhances CAR-T cell anti-tumor function in vivo.

A. NSG mice were injected intravenously with 1×10^6 Nalm6 leukemia cells. Three days later 2×10^6 of mock or HA-CAR-T cells manufactured in different media from day 6 to 10, were given intravenously.

B. Survival curves were compared using the log-rank Mantel–Cox test.

C. Tumor progression was monitored using bioluminescent imaging. Data are mean ± s.e.m. of n=5 mice per group. P values determined at day 21 by using Mann-Whitney test. (Right)

D. NSG mice were injected intravenously with 1×10^6 Nalm6 leukemia cells. Three days later 0.2×10^6 of mock or CD19-CAR-T cells manufactured in the presence of inosine or glucose, were given intravenously.

E. Tumor progression was monitored using bioluminescent imaging. Data are mean ± s.e.m. of n=10 mice per group.

F. NSG mice were inoculated with 1×10^6 143B osteosarcoma cells via intramuscular injection. At day 4 post-engraftment 1×10^7 mock or Her2.bbz-CAR-T cells cultured in glucose- or inosine-containing media were given intravenously.

G. 143B tumor growth monitored by caliper measurements. P values determined by unpaired two-tailed t-test with Welch's correction at day 20. (Right) Long-term survival of CAR-treated mice. Data are mean ± s.e.m. of n=3–5 mice per group.

H. Survival curves were compared using the log-rank Mantel–Cox test.

I. Concentration of total $CD3^+$ T cells detected in blood of mice at day 17 post-CAR-T cell injection.

P values determined by unpaired two-tailed t-test with Welch's correction.

J. *, $P < 0.05$; **, $P < 0.01$; ***, $P < 0.001$; ****, $P < 0.0001$.

See also Figure S5.

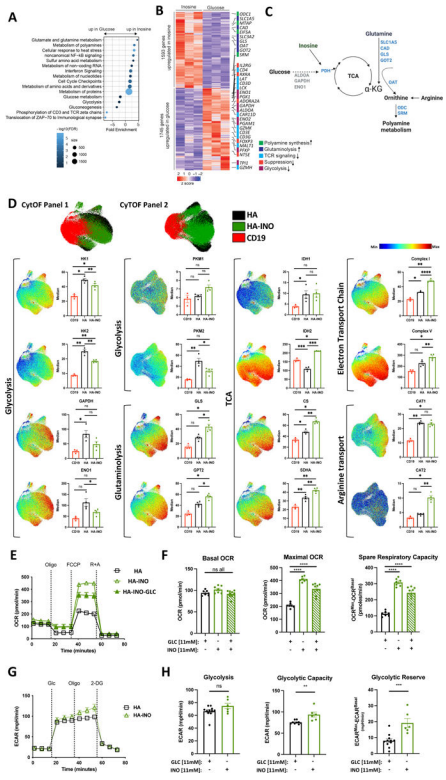

Figure 5: Exhausted CAR T cells expanded in inosine undergo metabolic reprogramming.

A. Pathway Enrichment Analysis of day 14 CAR-T cells shown in (3B) using the Reactome pathway collection and DAVID algorithm. Fold enrichment, number of genes represented, and FDR are shown.

B. Heat map of differentially expressed genes in HA- vs. HA-INO-CAR-T cells shown in (3B) (padj<0.01).

C. Graphic illustration of metabolic changes upon inosine addition into glucose-free culture media. Upregulated genes highlighted in (B) shown in blue and downregulated genes shown in grey.

D. UMAP analysis of $CD8^+$ CD19-, HA- or HA-INO-CAR T cells 14 days post-activation. Expression of 28 markers (Panel 1) or 24 markers (Panel 2) was analyzed by CyTOF. 9,000 of $CD8^+$ CAR-T cells from each condition and donor (n=3–4) were combined and colored by marker intensity. Graphs represent median expression of indicated markers expressed by $CD8^+$CAR-T cells. P values determined by paired two-tailed t-tests.

E. E-H. Seahorse analysis of mitochondrial fitness and glycolytic function was performed at day 11 post-activation.

F. Oxygen consumption rate (OCR) before and after treatment with oligomycin (Oligo), FCCP, and rotenone and antimycin (R+A). Plot shows mean ±s.e.m from 7–9 technical replicates from one representative donor (n=3).

G. Basal OCR, Maximal OCR and Spare Respiratory Capacity (SRC) from one representative donor. P values determined by two-way ANOVA with Dunnett's multiple comparisons test or Mixed-effects model with Dunnett's multiple comparisons test.

G. Extracellular acidification rate (ECAR) before and after treatment with glucose (Glc), oligomycin (Oligo), and 2-DG. Plot shows mean ±s.e.m from 6–9 technical replicates from one representative donor (n=5).

H. Basal Glycolysis, Glycolytic Capacity and Glycolytic Reserve from one representative donor. P values determined by paired two-tailed t-tests.

*, $P < 0.05$; **, $P < 0.01$; ***, $P < 0.001$; ****, $P < 0.0001$.

See also Figure S6.

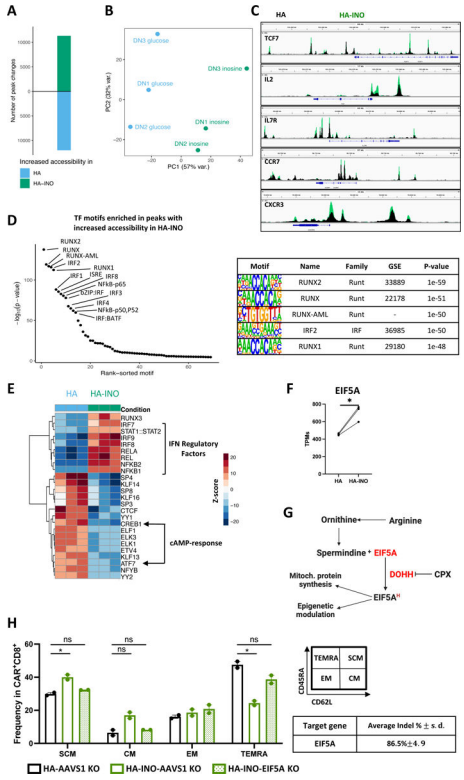

Figure 6. Inosine induces epigenetic reprogramming HA-CAR-T cells epigenetic by increasing polyamine metabolism.

A. Global chromatin accessibility profile of D14 $CD8^+$ HA- and HA-INO-CAR-T cells from three healthy individuals determined by ATAC-seq (p-value < 0.001 and log2 FC > 1).

B. PCA of ATAC-seq chromatin accessibility from HA-CAR-T cells cultivated in glucose or inosine.

C. Overlayed accessibility profiles in HA (black) and HA-INO-CAR-T cells (green) in the *TCF7, IL2, IL7R, CCR7* and *CXCR3* loci at day 14 post-activation. Concatenated samples from n=3 donors.

D. Top transcription factor motifs enrichment in HA-INO- vs HA-CAR-T cells ranked by HOMER analysis.

E. Top 25 transcription factor motif deviation scores in HA-INO- vs HA- by chromVAR analysis. Heatmap represents transcription factor deviation score.

F. Levels of expression of EIF5A gene transcripts from bulk RNA samples shown in (Fig. 4B). Data are mean+/− s.e.m. from n=3 donors. P values determined by paired two-tailed t-tests.

G. Graphic illustration of targeting polyamine-hypusine circuit. EIF5A- Eukaryotic initiation factor 5A; DOHH- Deoxyhypusine Hydroxylase; CPX- ciclopirox.

H. Relative frequency of stem cell memory ($CD45RA^+CD62L^+$), central memory (CM; $CD45RA^-CD62L^+$), effector memory (EM; $CD45RA^-CD62L^-$) and terminally differentiated effector (TEMRA; $CD45RA^+CD62L^-$), in control AAVS1-, EIF5A-KO $CD8^+$HA- or HA-INO-CAR-T cells at day 15 post-activation and measured by flow cytometry. (Right) CRISPR efficiency of indicated genes measured as Inference of CRISPR

Edits (ICE). Data are mean+/− s.e.m. from n=2 donors. P values determined by paired two-tailed t-tests.

*, $P < 0.05$; **, $P < 0.01$; ***, $P < 0.001$; ****, $P < 0.0001$.

See also Figure S7.

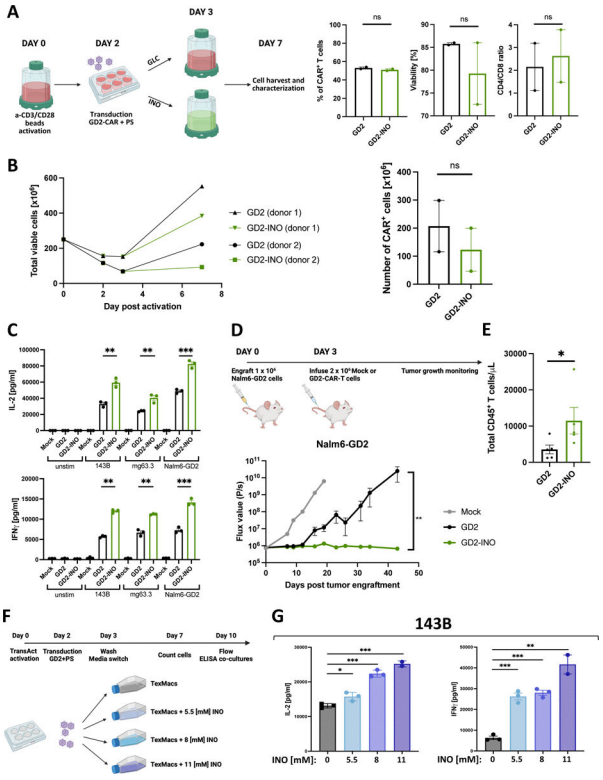

Figure 7. Clinical scale manufacturing of GD2-CAR-T cells using INO containing media improves CAR product quality.

A. Schematic of large-scale manufacturing of GD2.bbz-CAR^{-}T cells in a semi-closed G-Rex system in glucose- or inosine-containing media. 7 days post-activation, transduction efficiency, percentage of viable cells, and CD4/CD8 ratio of GD2^{+} cells were assessed by flow cytometry. Data are mean+/− s.e.m. from n=2 donors. P values determined by paired two-tailed t-tests.

B. (Left) Expansion of total viable T cells manufactured in control (black) vs. inosine (green)- containing media and (Right) corresponding number of CAR^{+} cells at day 7. Data are mean+/− s.e.m. from n=2 donors. P values determined by paired two-tailed t-tests.

C. IL-2 and IFNγ secretion by CAR-T cells stimulated for 24hrs with 143B, mg63.3 or Nalm6-GD2 tumor lines. Error bars represent mean ± SD of triplicate wells from one representative donor (n=2 donors). P values determined by unpaired two-tailed t-tests.

D. NSG mice were injected with 1×10^{6} Nalm6 leukemia cells. On day 3 post-tumor injection, 2×10^{6} of mock or GD2.bbz-CAR-T cells manufactured in the presence of inosine or in regular media were transferred intravenously. Tumor growth was monitored by bioluminescent imaging. Data are mean ± s.e.m. of n=5 mice per group. P values determined at day 43 by using Mann-Whitney test. Representative results of two independent experiments shown.

E. Concentration of CD45^{+} T cells detected in blood of mice at D32 post-CAR-T cell injection. P values determined by unpaired two-tailed t-test with Welch's correction. Results from one experiment shown.

F. Schematic of the experimental design.

G. GD2.bbz-CAR-T cells grown in media containing indicated inosine concentration between day 3 and day 10 post-activation and stimulated with 143B tumor. IL-2 and IFNγ secretion after 24hrs of co-culture was measured. Data are mean ± s.d. of duplicate or triplicate wells. Representative of n=3 donors shown. P values determined by unpaired two-tailed t-tests.

*, $P < 0.05$; **, $P < 0.01$; ***, $P < 0.001$; ****, $P < 0.0001$

See also Figure S8.

KEY RESOURCES TABLE

	SOURCE	IDENTIFIER
Antibodies		
FMC63-anti-idiotype (Dylight650 labelled)	Dr. Laurence Cooper, MD Anderson Cancer Center	N/A
1A7 anti-14G2a idiotype (Dylight650 labelled)	NCI Frederick and University of Texas M.D. Anderson Cancer	N/A
human Her2-Fc recombinant proteins (Dylight650 labelled)	R&D Systems	Cat#1129-ER-050
Human CD95-BV421 (clone DX2)	BioLegend	Cat#305624; RRID: AB_2561830
human CD4-APC-Cy7 (clone OKT4)	BioLegend	Cat#317418
human CD8-PerCp-Cy5.5 (clone SK1)	BioLegend	Cat#344709
human CD8-PE (clone SK1)	BioLegend	Cat#344706
human CD4-PE (clone OKT4)	BioLegend	Cat#317410
human TIM-3-BV510 (clone F38–2E2)	BioLegend	Cat#345030
human CD39-FITC (clone A1)	BioLegend	Cat#328205
human CD39-PE (clone A1)	BioLegend	Cat#328207
human CD39-APC-Cy7 (clone A1)	BioLegend	Cat#328225
HA.11 Epitope Tag- PE (clone 16B12)	eBioscience	Cat#901518
human CD73-PE-Cy7 (clone AD2)	eBioscience	Cat#25-0739-42; RRID: AB_2573368
human PD-1-PE-Cy7 (clone eBio J105)	eBioscience	Cat#25-9985-82; RRID: AB_10853805
human LAG-3-PE (clone 3DS223H)	eBioscience	Cat#12-2239-42; RRID: AB_2572597
human CD45RO-PE-Cy7 (clone UCHL1)	eBioscience	Cat#25-0457-42, RRID: AB_10718534
human CD45-PerCp-Cy5.5 (clone HI30)	eBioscience	Cat#45-0459-42; RRID: AB_10717530
human CCR7-PE (clone 3D12)	eBioscience	Cat#12-1979-42; RRID: AB_10670625
human CD3-BUV496 (clone UCHT1)	BD	Cat#612940
human LAG-3-BV421 (clone T47-530)	BD	Cat#565720; RRID: AB_2744330
human CD45RA-FITC (clone HI100)	BD	Cat#561882; RRID: AB_395879
human CD45RA-BV711 (clone HI100)	BD	Cat#563733; RRID: AB_2738392
human CD62L-BV605 (clone DREG-56)	BD	Cat#562719; RRID: AB_2744441
human CD73-BV510 (clone AD2)	BD	Cat#563198; RRID: AB_2738062
human CD4-BUV395 (clone SK3)	BD	Cat#563552; RRID: AB_2738273
Human CD8-BUV805 (clone SK1)	BD	Cat#612889; RRID: AB_2833078
CD278 (clone DX29)	BD	Cat#557801
CD226 (clone 11A8)	BioLegend	Cat#302839
CD69 (clone FN50)	BioLegend	Cat#310939
CD62L (clone DREG-56)	BioLegend	Cat#104443
CD4 (clone RPT-T4)	Fluidigm	Cat#3145001B
CD8 (clone RPT-T8)	Fluidigm	Cat#3146001B
CD28 (clone CD28.2)	BioLegend	Cat#302937
CD274 2(clone 9E.2A3)	Fluidigm	Cat#3148017B

	SOURCE	IDENTIFIER
CD45RO (clone UCHL1)	Fluidigm	Cat#3149001B
CD134 (clone ACT35)	Fluidigm	Cat#3150023B
CD49 (clone P1E6-C5)	BioLegend	Cat#329502
CD38 (clone HIT2)	BioLegend	Cat#303535
TIM-3 (clone F38-2E2)	Fluidigm	Cat#3153008B
TGIT (clone MBSA43)	Fluidigm	Cat#3154016B
cPARP (clone F21-852)	BD	Cat#552597
CD73 (clone AD2)	BioLegend	Cat#344002
CD25 (clone M-A251)	BioLegend	Cat#356102
CD137 (clone 4B4-1)	Fluidigm	Cat#3158013B
LAP (clone TW4-6H10)	BioLegend	Cat#349702
IL-10 (clone JES3-9D7	Biolegend	Cat#501423
Tbet (clone 4B10)	Fluidigm	Cat#3160010B
CD152 (clone 14D3)	Fluidigm	Cat#3161004B
Foxp3 (clone PCH101)	Invitrogen	Cat#14-4776-82
CD272 (clone MIH26)	Fluidigm	Cat#3163009B
CD39 (clone A1)	BioLegend	Cat#328221
CD223 (clone 874501)	Fluidigm	Cat#3165037B
CD101 (clone G043H7	Fluidigm	Cat#14-1019-82
CD197 (clone G043H7)	Fluidigm	Cat#3167009A
CD127 (clone A019D5)	Fluidigm	Cat#3168017B
CD45RA (clone HI100)	Fluidigm	Cat#3170010B
Ki67 (clone Ki67)	Biolegend	Cat#350523
CD122 (clone TU27)	Biolegend	Cat#339015
CD304 (clone 12C2)	Biolegend	Cat#305631
CD279 (clone EH12.2H7)	Fluidigm	Cat#3174020B
Helios (clone 22F6)	BioLegend	Cat#682602
EOMES (clone WD1928)	Biolegend	Cat#14-4877-82
TCF1 (clone C63D9)	Cell Signaling	Cat#2203S
CD27 (clone 323)	BioLegend	Cat#302802
CD95 (clone 305631)	BioLegend	Cat#305631
TOX (clone 6E6D03)	BioLegend	Cat#682602
LEF1 (clone C12A5)	Cell Signaling	Cat#2230S
PKM2 (clone D78A4)	Cell Signaling	Cat#4053S
PKM1	Thermo	Cat#15821-1-AP
BCAT1 (clone OTI3F5)	Thermo	Cat#CF504360
BCAT2 (clone 7G3A11)	Novus	Cat#NBP2-61699
ENO1 (clone EPR10863(B))	Abcam	Cat#ab206120
SDHA (clone 2E3GC12FB2AE2)	Abcam	Cat#ab14715

	SOURCE	IDENTIFIER
CS (clone EPR8067)	Abcam	Cat#ab233838
IDH1 (clone MAB7049)	R&D	Cat#843219
IDH2 (clone EPR7577)	Abcam	Cat#ab230796
GLS	LS BIO	Cat#LS-C166517-200
Glut1 (clone EPR3915)	Abcam	Cat#ab252403
GPT2	Proteintech	Cat#16757-1-AP
ATPA5 (clone 15H4C4)	Abcam	Cat#ab14748
NDUFB8 (clone 20E9DH10C12)	Thermo	Cat#459210
Bacterial and virus strains		
Stellar Competent Cells	Clontech, Takara	Cat# 636766
Biological samples		
Buffy Coats	Stanford Blood Bank	N/A
Whole Blood Samples of healthy donors	Stanford Blood Bank	N/A
Leukopaks from healthy donors	STEMCELL Technologies	N/A
Chemicals, peptides, and recombinant proteins		
Phusion Hot Start Flex 2X Master Mix	New England Biolabs	Cat# M0536L
Cisplatin	Fluidigm	Cat# 201064
Fixable Viability Dye eFluorÔ 450	Thermo Fisher	Cat# 65-0863-18
Fixable Viability dye eFluor780	Thermo Fisher	Cat# 65-0865-14
DNA intercalator	Fluidigm	Cat# 201191B
Rapid DNA Ligation Kit	Roche	Cat# 11-635-379-001
In-fusion HD Cloning System	Clontech, Takara	Cat# 639647
ZymoPURE II Plasmid Maxiprep Kit	Zymo Research	
Dynabeads Human T-Expander CD3/CD28	Thermo Fischer Scientific, Gibco	Cat# 11141D
Lipofectamine 2000 Transfection Reagent	Thermo Fischer Scientific	Cat# 11668500
RetroNectin Recombinant HumanFibronectin Fragment	Takara	Cat# T100B
Dylight 650 Micoscale Antibody Labelling Kit	Thermo Fischer Scientific	Cat# 84536
BD QuantiBRITE PE Beads	BD Biosciences	Cat# 340495
Recombinant Human IL-2	Preprotech	Cat# 200-02-1mg
Human IL-7	Miltenyi Biotec	Cat# 130-095-367
Human IL-15	Miltenyi Biotec	Cat# 130-095-760
Human Male AB Plasma-Derived Serum, Heat Inactivated (Human Thrombin)	Access Biologicals	Cat# 535-Hl
CryoStor CS10	STEMCELL Technologies	Cat# 07930
Alt-R.Sp. Cas9 protein	IDT	Cat# 1072532
CPI444	CORVUS BIOPHARMA	N/A
NECA	Torcis	Cat# 1691
ATPlite Luminescence Assay System	PerkinElmer	Cat# 6016941
Adenosine Assay Kit (Fluorometric)	Abcam	Cat# ab211094
Ciclopirox (CPX)	Sigma-Aldrich	SML2011

	SOURCE	IDENTIFIER
Critical commercial assays		
RNEasy Plus mini-isolation	Qiagen	Cat# 74134
CliniMACS CD8 GMP MicroBeads	Miltenyi Biotec	Cat# 170-076-703
CliniMACS CD4 GMP MicroBeads	Miltenyi Biotec	Cat# 170-076-702
RosetteSep Human T Cell Enrichment Cocktail	STEMCELL Technologies	Cat# 15061
SepMate-50 Tubes	STEMCELL Technologies	Cat# 85450
Human IFN-g ELISA MAX Deluxe	BioLegend	Cat# 430104
Human IL-2 ELISA MAX Deluxe	BioLegend	Cat# 431804
anti-PE MicroBeads	Miltenyi Biotec	Cat# 130-048-801
APC BrDU kit	BD	Cat# 552598
Annexin V Apoptosis Detection Kits	eBioscience	Cat# 88-8102-72
Seahorse XF Cell Mito Stress Test Kit	Agilent Technologies	Cat# 103015-100
Seahorse XF RPMI medium, without phenol red	Agilent Technologies	Cat# 103576-100
Seahorse XF Glycolysis Stress Test Kit	Agilent Technologies	Cat# 103020-100
P3 Primary Cell 4D-Nucleofector X Kit S	Lonza	Cat# V4XP-3032
Cell-Tak	Corning	Cat# CB-40240
Buffer PB	Qiagen	Cat# 19066
MinElute PCR Purification Kit	Qiagen	Cat# 28004
Index Kit 1 for Illumina	ApexBio	Cat# K1058
CountBright Absolute Counting beads	ThermoFisher	Cat# C36950
FACS Lysing Solution 10x	BD	Cat# 349202
Deposited data		
Bulk RNAseq data from CD4+ or CD8+ CD39+ vs CD39-	This paper	GSE250442
Bulk RNAseq data from AAVS1KO, CD39KO, CD73KO, A2aR KO, ADA-OE HA-CAR T cells	This paper	GSE250442
Bulk RNAseq data from HA-CAR T cells cultured in glucose- vs inosine-containing media	This paper	GSE250442
ATACseq from HA-CAR T cells cultured in glucose- vs inosine-containing media	This paper	GSE250439
Experimental models: Cell lines		
143B	ATCC	Cat# CRL-8303
Nalm6	Dr. David Barrett (Children's Hospital of Philadelphia)	N/A
Nalm6-CD19low	Dr. Robbie Majzner (Dana Faber Cancer Insititute)	N/A
MG63.3	Chand Khanna (National Cancer Institute, National Institutes of Health	N/A
Experimental models: Organisms/strains		
Mice: NSG (NOD.Cg-Prkdcscid Il2rgtm1Wjl/SzJ)	The Jackson Laboratory	Cat# JAX:005557; RRID:IMSR JAX:005557
Oligonucleotides		
AAVS1-GGGGCCACTAGGGACAGGAT	Synthego	N/A

	SOURCE	IDENTIFIER
ADORA2a-guide1-GUCUGUGGCCAUGCCCAUCA	Synthego	N/A
ADORA2a-guide2-UACACCGAGGAGCCCAUGAU	Synthego	N/A
CD73-guide1-GCGGGCGCCCGCGCGGCUCG	Synthego	N/A
CD73-guide2-CUAUGUGUCCCCGAGCCGCG	Synthego	N/A
CD39-UGGCACCCUGGAAGUCAAAG	Synthego	N/A
EIF5A-UACAUACAGGUCCAUCUGGU	Synthego	N/A
Recombinant DNA		
RD 114	previously used in our lab	N/A
CAR.CD19.FMC63.8aHTM.BBz	previously used in our lab	N/A
CAR.CD19.FMC63.28TM.28z	previously used in our lab	N/A
CAR.HER2.4D5.8aHTM.BBz	previously used in our lab	N/A
CAR.GD2.14g2a-E101K.28TM.28z	previously used in our lab	N/A
ADA1.HA. 8aHTM	This manuscript	N/A
Software and algorithms		
FlowJo v10.7.1	FlowJo, LLC	N/A
GraphPad Prism v8.4	GraphPad Software Inc.	N/A
Living Image version (IVIS imaging)	Perkin Elmer	N/A
Biorender	Biorender	N/A
OMIQ	OMIQ	N/A
DESeq2 v1.30.1	Ref# 70	N/A
IGV v1.9.0	Ref# 69	N/A
ComBat_seq	Ref# 71	N/A
chromVAR v1.12.0	Ref# 72	N/A
Seahorse Wave Pro	Agilent	N/A
OMIQ	OMIQ	N/A
Salmon	Salmon	salmon.html
SnapGene v5.2.3	SnapGene v5.2.3	N/A
Other		
Incucyte ZOOM	Sartorius	
BD LSRFortessaÔ X-20	BD Biosciences	
Beckman CytoFLEX analyzer	Beckman Coulter	
T Cell TransAct™, human	Miltenyi Biotec	Cat# 130-111-160
Protamine sulfate	Frezenius-Cabi	N/A